Criegee Intermediates: Production, Detection and Reactivity

Rabi Chhantyal-Pun[1*], M. Anwar H. Khan[1*], Craig A. Taatjes[2], Carl J. Percival[3], Andrew J. Orr-Ewing[1], Dudley E. Shallcross[1]

[1]School of Chemistry, University of Bristol, Cantock's Close, Bristol BS8 1TS, UK.

[2]Combustion Research Facility, Mailstop 9055, Sandia National Laboratories, Livermore, California, 94551 USA.

[3]Jet Propulsion Laboratory, California Institute of Technology, 4800 Oak Grove Dr, Pasadena, CA 91109, USA

*Author to whom correspondence should be sent

E-mail: rc13564@bristol.ac.uk, rcpchem@gmail.com (R. Chhantyal-Pun), anwar.khan@bristol.ac.uk (M.A.H. Khan)

Abstract

In the context of tropospheric chemistry, Criegee intermediates denote carbonyl oxides with biradical / zwitterionic character (R_1R_2COO) that form during the ozonolysis of alkenes. First discovered almost 70 years ago, stabilized versions of Criegee intermediates formed via collisional removal of excess energy have interesting kinetic and mechanistic properties. The direct production and detection of these intermediates were not reported in the literature until 2008. However, recent advances in their generation through the ultraviolet irradiation of the corresponding diiodoalkanes in excess O_2 and detection by various spectroscopic techniques (photoionization, ultraviolet, infrared, microwave and mass spectrometry) have shown that these species can react rapidly with closed shell molecules, in many cases at or exceeding the classical gas-kinetic limit, via multiple reaction pathways. These reactions can be complex, and laboratory measurements of products and the temperature and pressure dependence of the reaction kinetics have also revealed unusual behaviour. The potential role of these intermediates in atmospheric chemistry is significant, altering models of the oxidising capacity of the Earth's atmosphere and the rate of generation of secondary organic aerosol.

Keywords: Criegee Intermediates, Reaction Mechanisms, Atmospheric Chemistry

1. Background to Criegee intermediates

Alkene ozonolysis reactions are widely accepted to proceed via the Criegee mechanism [1]. On addition of ozone to an alkene, a primary ozonide is formed which undergoes rapid

exothermic decomposition to form a carbonyl oxide (referred to as a Criegee intermediate) and a stable carbonyl compound, as shown in Scheme 1. The decomposition products of the ozonide depend upon the substitution of the alkenes. This exothermic decomposition generates a substantial amount of vibrational excitation in the Criegee intermediate. This internal energy enables further rapid unimolecular loss, often yielding hydroxyl radicals (OH), in competition with collisional quenching in ambient air to produce stabilized Criegee intermediates (sCIs) that can undergo slower isomerization or fragmentation. However, sCIs remain reactive because of their biradical/zwitterion character and have a sufficiently long lifetimes to undergo bimolecular reactions with atmospheric trace gases [2-5]. Different sCIs may have substantially different reactivity, which is demonstrated by experimental studies of their chemistry [6-13].

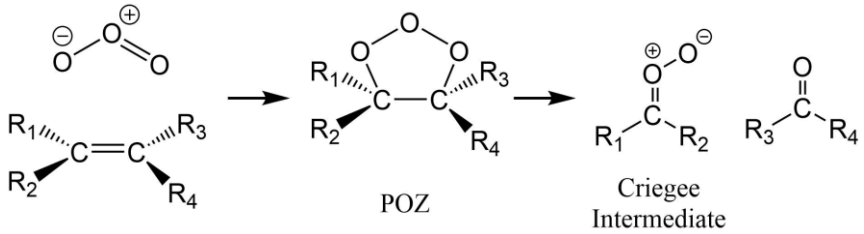

Scheme 1. Ozonolysis of alkene generating primary ozonide (POZ) which dissociates to form a Criegee intermediate and a carbonyl compound.

For many years, the existence of sCIs was inferred through indirect experimental evidence in numerous laboratory studies [9, 10, 14-17], from which estimates were made of reaction rate coefficients. In many cases, the analysis of such measurements relied on kinetic models, which increases uncertainties in the rate coefficient determinations. In 2008, the simplest sCI, CH_2OO, was generated directly and detected [18], and in 2012 a method was discovered to generate more substantial concentrations of sCI, allowing direct time resolved kinetic studies to be performed [2, 3, 19]. These direct studies suggested that sCIs reacted far more rapidly than had previously been appreciated with a wide range of species in the atmosphere, and that for some of these trace atmospheric constituents sCIs could be a key reaction partner. The first direct experimental detection of CH_2OO in the gas-phase ozonolysis of ethylene was reported by McCarthy and co-workers in 2015 using Fourier Transform microwave spectroscopy coupled with a pulsed nozzle expansion [20]. Recently, Berndt et al. [21] reported direct and sensitive detection of steady state sCI from the ozonolysis of alkenes in a free-jet flow system by means of chemical ionization mass spectrometry, with a detection limit of ~10^4 – 10^5 molecule cm^{-3}, approaching the sensitivities required for direct tropospheric detection.

Earlier reviews by Osborn and Taatjes [22], Y. P. Lee [23] and Lin and Chao [24], and Taatjes [25] have highlighted the advances in direct detection and production methods of the sCIs as well as spectroscopy and reactivity of the simpler sCIs. Reviews by Taatjes and Khan et al. have focused on reactivity of Criegee intermediates and their impacts on the troposphere [25, 26]. A further article by Lester and Klippenstein [27] described the unimolecular dissociation dynamics of Criegee intermediates to produce OH radical. Here, we focus on recent advances in the methods to generate sCIs, detect them in the laboratory, and study their gaseous reactions to learn about reaction pathways, transition states, transient intermediates, and reaction products.

2. Production of Criegee intermediates

Until recently, laboratory measurements extensively used ozonolysis of alkenes, as shown in Scheme 1, to produce sCI and infer their reactivity [28]. Various scavengers such as SO_2, H_2O, organic acids and carbonyl compounds were employed during ozonolysis experiments, and resulting changes in final product yields used to estimate stabilization of Criegee intermediates along the reaction pathway. The sCI yields are variable because their formation depends on the temperature, pressure, and the nature of the substituents of the reactant alkenes [29, 30].Theoretical and indirect experimental studies have reported a range of sCIs yields for different alkenes, as summarized in Table 1.

Table 1. Yield of stabilized Criegee intermediates from ozonolysis of alkenes.

Alkenes	sCI yield	Conditions (T/K, p)	sCI scavenger	References
Ethene	0.59 ± 0.17	298K and 1 atm	CH_3COOH	Yajima et al. [31]
	0.39 ± 0.05	298K and 1 atm	SO_2	Hatakeyama et al. [32]
	0.39 ± 0.11	298K and 1 atm	H_2O	Hasson et al. [33]
	0.54 ± 0.12	298K and 1 atm	CO	Alam et al. [34]
	0.40-0.50	295K and 730 Torr	HCOOH, CH_3COOH,	Neeb et al. [35]
	0.50± 0.04	296K and 730 Torr	CH_3OH	Neeb et al. [36]
	0.52± 0.06	295K and 730 Torr	CF_3COCF_3	Horie et al. [37]
	0.35 ± 0.05	298K and 700 Torr	CF_3COCF_3, CH_3CHO	Niki et al. [38]
	0.37 ± 0.02	282-303K and 700 Torr	HCHO	Kan et al. [39]
	0.38 ± 0.06	291-299K and 700 Torr	HCHO	Su et al. [40]
	0.47	297K and 758 Torr	HCHO	Horie and Moortgat [10]
	0.40 ± 0.18	293K and 1 atm	SO_2	Berndt et al. [41]
	0.42	293K and 730 Torr	H_2O	Neeb et al. [[42]
	0.37 ± 0.04	296-303K and 1 atm	SO_2	Newland et al. [43]
	0.48 ± 0.05	300K and 1 atm	Theoretical	Nguyen et al. [44]
	0.21-0.29	300K and 1 atm	Theoretical	Olzmann et al. [16]
Propene	0.25-0.44		Review	Finlayson-Pitts and Pitts [45]
	0.22	296K and 1 atm	SO_2	Rickard et al. [9]
	0.25 ± 0.02	298K and 1 atm	SO_2	Hatakeyama et al. [15]
	0.14 (φCH_2OO)	293K and 730 Torr	H_2O	Neeb et al. [42]
Isobutene	0.17 ± 0.03	298K and 1 atm	SO_2	Hatakeyama et al. [15]
	0.13 (φCH_2OO)	293K and 730 Torr	H_2O	Neeb et al. [42]
1-Butene	0.27	298K and 1 atm	H_2O	Hasson et al.[46]

2-methyl-2-butene	0.10	296K and 1 atm	SO_2	Rickard et al. [9]
2,3-dimethyl-2-butene	0.62 ± 0.28	293K and 1 atm	SO_2	Berndt et al. [47]
	0.10 ± 0.03	298K and 1 atm	H_2O	Hasson et al. [46]
	0.30	298K and 700 Torr	HCHO	Niki et al. [48]
	0.11	296K and 1 atm	SO_2	Rickard et al. [9]
	0.29	295K and 730 Torr	CF_3COCF_3	Horie et al.[37]
	0.32 ± 0.02	296-303K and 1 atm	SO_2, H_2O	Newland et al. [43]
	0.45 ± 0.20	278-343K and 1 atm	SO_2	Berndt et al. [49]
	0.37 ± 0.02	298K and 900 Torr	SO_2	Hakala and Donahue [50]
	0.15 ± 0.02	298K and 50 Torr	SO_2	Hakala and Donahue [50]
trans-2-butene	0.28 ± 0.03	296-303K and 1 atm	SO_2, H_2O	Newland et al. [43]
	0.53 ± 0.24	293K and 1 atm	SO_2	Berndt et al. [47]
	0.49 ± 0.22	278-343K and 1 atm	SO_2	Berndt et al. [49]
	0.19-0.42		Review	Finlayson-Pitts and Pitts [45]
	0.19 ± 0.03	298K and 1 atm	SO_2	Hatakeyama et al. [15]
	0.24 ± 0.07	298K and 1 atm	H_2O	Hasson et al. [46]
	0.13	296K and 1 atm	SO_2	Rickard et al. [9]
	0.22	295K and 730 Torr	CF_3COCF_3	Horie et al. [37]
	0.42	297K and 758 Torr	HCHO	Horie and Moortgat [10]
	0.45	295K and 1 atm	SO_2	Cox and Penkett [51]
cis-2-butene	0.38 ± 0.05	296-303K and 1 atm	SO_2, H_2O	Newland et al. [43]
	0.19	296K and 1 atm	SO_2	Rickard et al. [9]
	0.18	298K and 760 Torr	HCHO	Niki et al. [52]
	0.43	295K and 1 atm	SO_2	Cox and Penkett [51]
Isoprene	0.58 ± 0.26	293K and 1 atm	SO_2	Sipilä et al. [53]
	0.56 ± 0.03	287-302K and 750 Torr	SO_2	Newland et al. [54]
	0.26	298K and 1 atm	H_2O	Hasson et al. [46]
	0.30 (φ_{CH_2OO})	293K and 730 Torr	H_2O	Neeb et al. [42]
	0.28	296K and 1 atm	SO_2	Rickard et al. [9]
1-Pentene	0.29	298K and 1 atm	H_2O	Hasson et al. [46]
cyclopenetene	0.05 ± 0.01	298K and 1 atm	SO_2	Hatakeyama et al. [15]
cyclohexene	0.03 ± 0.02	298K and 1 atm	SO_2	Hatakeyama et al. [15]
cycloheptene	0.03 ± 0.02	298K and 1 atm	SO_2	Hatakeyama et al. [15]
1-Octene	0.35	298K and 1 atm	H_2O	Hasson et al. [46]
	0.10 ($\varphi_{C7\text{-}SCI}$)	298K and 1 atm	Theoretical	Paulson and Seinfeld [55]
Methylene cyclohexane	0.18	298K and 1 atm	H_2O	Hasson et al. [46]
	0.22 ± 0.03	298K and 1 atm	SO_2	Hatakeyama et al. [15]
1-methyl-cyclohexene	0.16 ± 0.07	293K and 1 atm	SO_2	Berndt et al. [40]
	0.10 ± 0.07	298K and 1 atm	SO_2	Hatakeyama et al. [15]
α-pinene	0.15 ± 0.07	293K and 1 atm	SO_2	Sipilä et al. [53]
	0.13 ± 0.04	298K and 1 atm	SO_2	Hatakeyama et al. [15]
	0.19 ± 0.01	287-302K and 750 Torr	SO_2	Newland et al. [54]
	0.15	298K and 740 Torr	CF_3COCF_3	Drozd and Donahue [29]
	0.05	298K and 110 Torr	CF_3COCF_3	Drozd and Donahue [29]
	0.34	298K and 1 atm	Theoretical	Zhang and Zhang [56]
β-pinene	0.14	296K and 1 atm	SO_2	Rickard et al. [9]
	0.25± 0.02	298K and 1 atm	SO_2	Hatakeyama et al. [15]
	0.27	298K and 1 atm	H_2O	Hasson et al. [46]
	0.44	295-298K and 1 atm	SO_2	Kotzias et al. [57]
	0.27	295K and 1 atm	H_2O and CH_3COOH	Ma and Marston [58]
	0.60 ± 0.03	287-302K and 750 Torr	SO_2	Newland et al. [54]
	0.46 ($\varphi_{C9\text{-}SCI}$-0.36, φ_{CH2OO}-0.10)	298K and 340 Torr	SO_2	Ahrens et al. [59]
	0.51 ($\varphi_{C9\text{-}SCI}$-0.35, φ_{CH2OO}-0.16)	296K and 730 Torr	HCHO, HCOOH, H_2O	Winterhalter et al. [60]
	0.30 ($\varphi_{C9\text{-}SCI}$-0.22, φ_{CH2OO}-0.08)	298K and 1 atm	Theoretical	Zhang and Zhang [56]
	0.42 ($\varphi_{C9\text{-}SCI}$-0.37, φ_{CH2OO}-0.05)	298K and 1 atm	Theoretical	Nguyen et al. [61]
Limonene	0.27 ± 0.12	293K and 1 atm	SO_2	Sipilä et al. [53]

	0.23 ± 0.01	287-302K and 750 Torr	SO_2	Newland et al. [54]
Myrcene	0.30	287-302K and 750 Torr	SO_2	Newland et al. [54]
Ocimene	0.30	287-302K and 750 Torr	SO_2	Newland et al. [54]
styrene	0.26 ± 0.01	298K and 1 atm	SO_2	Hatakeyama et al. [15]
vinyl chloride	0.23 ± 0.03	298K and 1 atm	SO_2	Hatakeyama et al. [15]

The first direct detection of a stabilized Criegee intermediate labelled simply as a Criegee intermediate hereafter, was achieved by Taatjes et al. [18] using dimethyl sulphoxide ($CH_3S(O)CH_3$; DMSO) as a precursor to CH_2OO. In DMSO oxidation, the reaction of $CH_3S(O)CH_2$ with O_2 in a low-pressure flow cell produces CH_2OO. Criegee intermediate formation by this technique is an exothermic process with an energy release of 52.3 kJ mol^{-1} [62], which is small compared to the 200 to 250 kJ mol^{-1} exothermicity of formation from ozonolysis of ethene [30]. This method provided the first photolytic generation of gas-phase Criegee intermediates in sufficient yields to allow direct detection.

$$CH_3S(O)CH_3 + Cl \rightarrow CH_3S(O)CH_2 + HCl \quad (1)$$

$$CH_3S(O)CH_2 + O_2 \rightarrow CH_3S(O) + CH_2OO \quad (2)$$

However, the signal-to-noise ratio for detected CH_2OO was insufficient for kinetic experiments. Welz et al. [2] discovered a more efficient method for producing Criegee intermediates by the photolysis of diiodomethane (CH_2I_2) in the presence of excess molecular oxygen. The photolysis of CH_2I_2 produces an iodomethyl radical, CH_2I which reacts rapidly with O_2 through the competitive channels shown in 4a and 4b.

$$CH_2I_2 + h\nu \rightarrow CH_2I + I \quad (3)$$

$$CH_2I + O_2 \rightarrow CH_2OO + I \quad (4a)$$

$$CH_2I + O_2 \rightarrow CH_2IOO \quad (4b)$$

This production method has proved effective and been widely used by different groups for kinetic and spectroscopic measurements. It has been used to generate CH_2OO in both flow cell [2, 63-68] and molecular beam [69] experiments. A similar method with CH_2Br_2 has been used to generate CH_2OO in a plasma discharge [70]. Various other Criegee intermediates have been produced following analogous methods, but with a variety of gem-diiodide precursors, e.g., CH_3CHOO from CH_3CHI_2 [3, 19, 71-73] $(CH_3)_2COO$ from $(CH_3)_2CI_2$ [5, 74, 75], CH_3CH_2CHOO from $CH_3CH_2CHI_2$ [74]. At low pressure, the yield of R(4a) approaches unity, but CH_2IOO can be the dominant product at atmospheric pressure and at 295 K (approx. 80%)

although with a non-negligible branching ratio forming the Criegee intermediate [65, 76]. This technique may not be a viable route to higher Criegee intermediates (>C_3) because the low vapour pressure of the diiodide limits the gas-phase concentration that can be generated, and because the competing formation of the iodoperoxy radical may dominate. Barber et al. [77] recently generated methyl vinyl ketone oxide (MVKOO) Criegee intermediate by the photolysis of 1,3-diiodobut-2-ene at 248 nm in the presence of O_2 through the preferential dissociation of the weaker allylic C_1-I bond rather than the vinylic C_3-I bond, a consequence of the resonance stabilization of the allylic monoiodoalkenyl radical. Similarly, Vansco et al. [78] generated methacrolein oxide (MACROO) using 248 nm photolysis of (E)-1,3-diiodo-2-methylprop-1-ene in the presence of O_2. However, direct kinetic measurements of unimolecular and bimolecular reactions of MVKOO and MACROO Criegee intermediates have not yet been reported.

3. Detection of Criegee intermediates

Several spectroscopic methods have been used to detect Criegee intermediates following the methods of generation outlined in the previous section, and reviews can be found by Lee [23], Osborn and Taatjes [22], Taatjes et al. [79] and Taatjes [25]. Techniques that have been successfully used to detect gas phase Criegee intermediates include photoionization spectroscopy [2, 5, 19], ultraviolet spectroscopy [63, 64, 66-69, 80], infrared spectroscopy [59, 81, 82], microwave spectroscopy [70, 83] and submillimetre-wave spectroscopy [84]. Recently, mass spectrometric methods have also been developed to measure Criegee intermediates directly during ozonolysis experiments [21, 85].

The tuneable synchrotron photoionization mass spectrometry method used by Taatjes and co-workers allows the time resolved photoionization spectrum to be recorded for a specific mass channel. The initial observation of CH_2OO was confirmed by its photoionization spectrum with an onset of ~10 eV for a mass/charge (m/z = 46) species; ionization energies of other isomers at m/z = 46, such as dioxirane, methylene bis(oxy) and formic acid (see Figure 5 of Reference [22]) are substantially higher. The structure of the next in the series of Criegee intermediates, acetaldehyde oxide, CH_3CHOO, gives rise to *syn*- and *anti*-conformers with different ionization energies, and the *syn*- and *anti*-conformers of CH_3CHOO display different photoionization spectra (see Figure 1 of Reference [19]). The s*yn*-CH_3CHOO appears to be the dominant conformer observed, perhaps because of its lower energy. The difference in ionization energy of the two conformers can be used to separate their reactivity towards other

compounds (e.g. SO_2, H_2O, water dimer). The production of acetone oxide, $(CH_3)_2COO$, from the photolysis of $(CH_3)_2CI_2$ in the presence of O_2 has been confirmed by the photoionization spectrum collected for m/z = 74 species as shown in Figure 1. Figure 1 shows a best fit of the m/z =74 ion yields in the ionization threshold region (<9.5 eV) to a combination of Franck-Condon factor weighted photoionizations from the ground neutral state to the two lowest states of the $(CH_3)_2COO^+$ ion. The ionization energies of different Criegee intermediates measured at room temperatures are provided in Table 2. Photoionization mass spectrometry has also been used to characterize the kinetics and products of Criegee intermediates reactions, as described in detail in the next section.

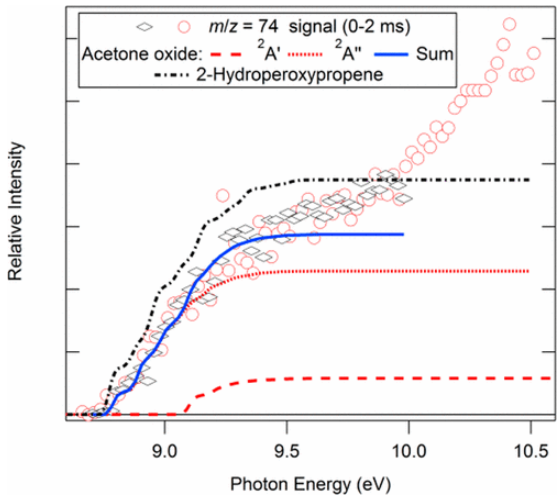

Figure 1. The photoionization spectrum for the m/z 74 product (possibly $(CH_3)_2COO$) from the photolysis of the gem-diiodide $(CH_3)_2CI_2$ in the presence of O_2. Calculated Franck Condon envelopes for ionization of $(CH_3)_2COO$ to two cationic states and of 2-hydroperoxypropene are shown by the dotted traces. The blue trace shows the best fit of the combined $(CH_3)_2COO$ envelopes to the experimental trace. Figure reprinted from Reference [5] with permission from the American Chemical Society.

Table 2. Ionization energies for different Criegee intermediates at ambient conditions.

Criegee Intermediate	Ionization energy	References
CH_2OO	~10 eV	Welz et al. [2]
syn-CH_3CHOO	~9.4 eV	Taatjes et al. [19]
anti-CH_3CHOO	~9.3 eV	Taatjes et al. [19]
$(CH_3)_2COO$	~8.8 eV	Chhantyal-Pun et al. [5]

The CH_2OO $B^1A' \leftarrow X^1A'$ absorption spectrum in the UV region was first obtained by measuring the UV-induced depletion of the vacuum UV (118 nm) photoionization signal at m/z=46 by Lester and co-workers under molecular beam conditions. Beames et al. [69] observed a broad and diffuse absorption peak in the region of 300-370 nm with a maximum near 335 nm. A subsequent direct absorption spectroscopy measurement by Sheps using a

broad-band UV light source [63] obtained a broader CH_2OO B-X spectrum with vibrational progression on the red side, analogous to the structured Huggins band in the isoelectronic O_3 spectrum, and a peak absorption around 355 nm. A further such measurement by Ting et al. [64] recorded a similar CH_2OO B-X spectrum to that of Sheps [63], exhibiting vibronic structures on the long-wavelength side but with some discrepancies in absorbance on the short-wavelength side of the band. However, the absorption cross-sections reported by Ting et al. [64] are three times lower than those measured by Sheps [63] (see Table 3). Ting et al. measured absolute absorption cross sections at 308.4 and 351.8 nm using a depletion method in molecular beam experiments and used those values to calibrate the ambient broadband spectrum as shown in Figure 2. The UV spectrum in the high energy region was expected to be similar under ambient and molecular beam conditions. The peak absorption cross sections and wavelengths measured for CH_2OO and other Criegee intermediates are given in Table 3. Foreman et al. [86] measured higher resolution spectra (~0.1 nm) in the longer wavelength region (362-470 nm) which were consistent with the broadband measurements. No significant temperature dependence was observed for the progression bands within the 276-357 K range. Thus, the vibronic structures likely arises from quasi bound vibrations in the excited state, as suggested by the computational study of Dawes et al. [87].

Table 3. Peak ultraviolent absorption cross sections for various Criegee intermediates. [a]Ambient conditions [b]Molecular beam condition.

Criegee intermediate	**Wavelength (nm)**	**Cross section (cm^2)**	**References**
CH_2OO	355[a] 340[a] 335[b]	$(3.6\pm0.9) \times 10^{-17}$ $(1.23\pm0.18) \times 10^{-17}$ $\sim5.0 \times 10^{-17}$	Sheps [80] Ting et al. [65] Beames et al. [62]
syn-CH_3CHOO	323[a] 328[a]	1.2×10^{-17} $(1.27\pm0.11) \times 10^{-17}$	Sheps et al. [67] Smith et al. [66]
anti-CH_3CHOO	360[a]	1.2×10^{-17}	Sheps et al. [67]
$(CH_3)_2COO$	320[b] 330[a]	4.0×10^{-17} $(1.75\pm0.14) \times 10^{-17}$	Liu et al. [73] Chang et al. [71]
CH_3CH_2CHOO	320[b]	4.0×10^{-17}	Liu et al. [73]

The CH_3CHOO (B-X) UV absorption spectrum was found by Smith et al. [71] to be narrower than that for CH_2OO and the peak is shifted by 14-15 nm to a shorter wavelength. Similar to CH_2OO, the UV depletion spectrum of CH_3CHOO reported by Beames et al. [73] under molecular beam conditions was narrower than the UV absorption spectrum measured by Smith et al. [71] under ambient condition. Sheps et al. [72] distinguished the spectra of the *syn*- and *anti*-conformers peaking around 320 and 370 nm, respectively, in the CH_3CHOO UV

absorption spectrum using the difference in reactivities of the two conformers with water. Chang et al. [88] measured the peak absorption wavelength for $(CH_3)_2COO$ to be at 330 nm which is blue shifted from the CH_2OO peak, and the maximum absorption cross section of $(CH_3)_2COO$ is larger than those of CH_2OO and CH_3CHOO (see Figure 2). Recently, Vansco et al. [78, 89] measured the UV spectra of methyl vinyl ketone oxide (MVKOO) and methacrolein oxide (MACROO) Criegee intermediates using the UV depletion method described earlier. The UV spectrum was found to be significantly red shifted, with depletion peaks at 388 (MVKOO) and 380 nm (MACROO), and cross sections in the region of ~10^{-17} cm^2. Various measurements of the Criegee intermediate absorption spectra discussed above are combined in Figure 2.

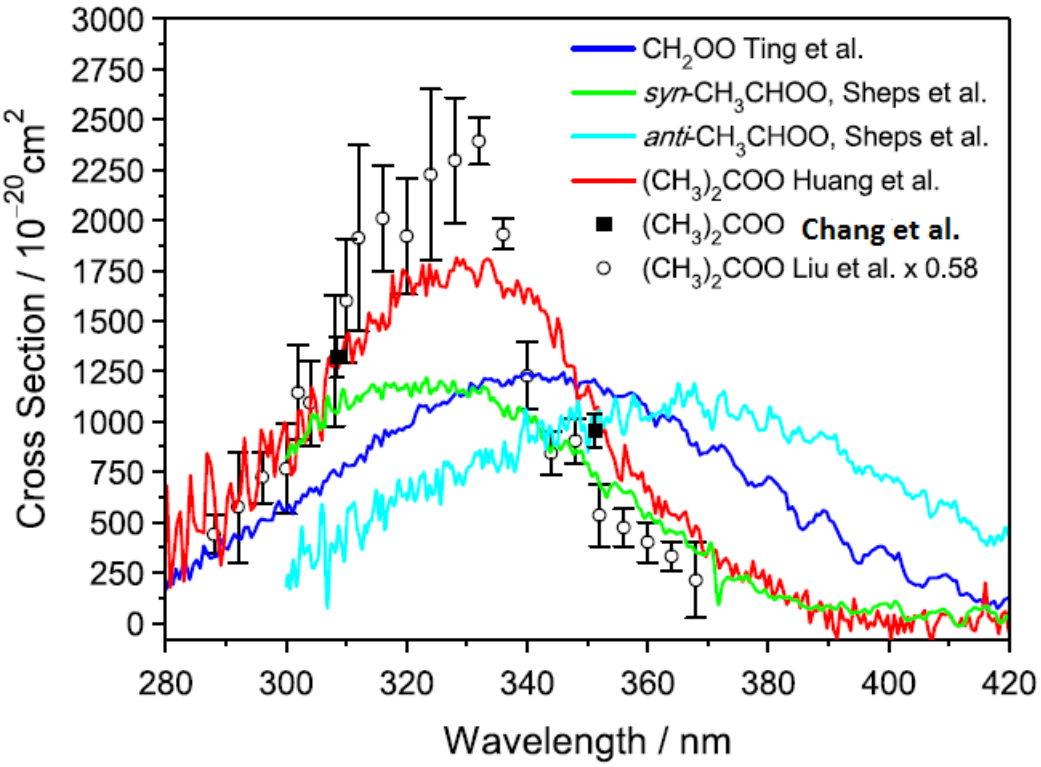

Figure 2. A comparison of UV absorption spectra of CH_2OO, syn-CH_3CHOO, anti-CH_3CHOO and $(CH_3)_2COO$ from different studies. Figure reprinted from Reference [88] with permission from Elsevier.

The large UV absorption cross sections offer sensitive optical probes of various Criegee intermediates and have now been used extensively to study time resolved reaction kinetics by various groups around the world. Lin and co-workers used multi-pass UV broadband absorption spectroscopy to measure broadband spectra and reaction kinetics of various Criegee intermediates at temperatures (~270 to 350 K) relevant in the troposphere [24]. Seakins and co-workers have used a similar setup to study the reaction kinetics of CH_2OO at ambient temperature [90]. Green and co-workers have used a multi-pass Herriott cell coupled with the

frequency doubled output of a picosecond Ti:Sapphire laser, tuned to produce 375 nm radiation, to probe reaction kinetics of CH_2OO at temperatures relevant in combustion systems (298 to 494 K) [91]. Murray and co-workers have used single pass UV broadband spectroscopy based on a LED light source to measure reaction kinetics of CH_2OO at ambient temperature [68]. Sheps and co-workers have used cavity enhanced absorption spectroscopy to measure broadband spectra and reaction kinetics of CH_2OO and CH_3CHOO at ambient temperature and temperatures relevant for combustion systems [72, 92]. Orr-Ewing and co-workers have used cavity ring-down absorption spectroscopy, coupled with the frequency doubled output of a Nd:YAG laser to produce 355 nm radiation, to measure reaction kinetics of CH_2OO and $(CH_3)_2COO$ at temperatures (~240 to 340 K) relevant in the troposphere [93, 94].

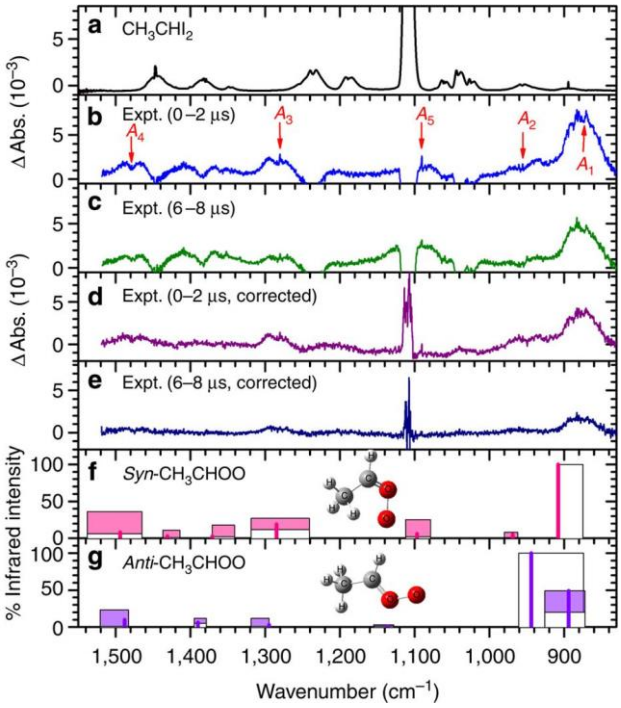

Figure 3. IR absorption spectra of CH_3CHI_2 in the presence of O_2 before photolysis (a) and after photolysis (b and c) along with the products assigned as syn- and anti- CH_3CHOO. Figure reprinted from Reference [95] with permission from Springer Nature.

The CH_2OO and CD_2OO infrared absorption spectra were measured by Lee and co-workers using a broadband time resolved step-scan FTIR spectrometer coupled with a multipass White cell [81, 96]. The transient infrared bands were assigned to CH_2OO based on agreement with calculated vibrational frequencies and rotational band contours. Infrared absorption spectra of CH_3CHOO, shown in Figure 3, and $(CH_3)_2COO$ have since been measured using the same set up [95, 97]. The vibrational band positions and assignments are summarised in Table 4. Ahrens et al. [59] measured infrared bands between 930 and 830 cm^{-1} of Criegee intermediates formed during ozonolysis of β-pinene under dry conditions. The broadband step-scan FTIR

spectroscopy method has also been applied to characterize products from the reactions of Criegee intermediates, as is described in detail in the next section. A rotationally resolved infrared spectrum (0.0015 cm^{-1} resolution) of the O-O stretch band centred around 908 cm^{-1} , shown in Figure 4**Table *4***, was measured for CH_2OO using a continuous wave quantum cascade laser (CW-QCL) by the same group [98]. Lin and co-workers also used CW-QCL spectroscopy to obtain a rotationally resolved (0.002 cm^{-1} resolution) infrared spectrum of the CH_2OO CO stretch/CH_2 scissor vibrational band centred around 1285 cm^{-1} and used it to determine a rate coefficient for reaction of CH_2OO with O_3 [99]. High-resolution infrared spectroscopy provides an alternative to UV absorption spectroscopy for interference-free measurement of Criegee intermediate reaction kinetics [99, 100]. Lester and co-workers have used action spectroscopy to measure infrared spectra and unimolecular reaction kinetics of various Criegee intermediates with α-hydrogen atoms [112-114] examples of which are described in the next section.

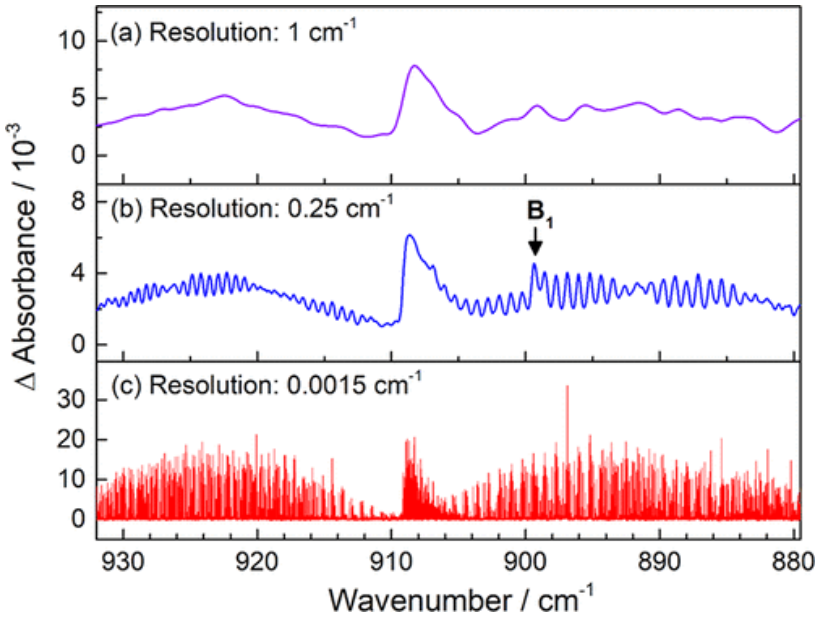

Figure 4. (a) Observed spectra of CH_2OO at various spectral resolutions (1 - 0.0015 cm^{-1}) in the region of 880-932 $cm^{-1}$and (b) partial spectra of syn-CH_3CHOO at a resolution of 0.0015 cm^{-1}. Figure reprinted from Reference [98] with permission from the American Chemical Society.

Table 4. Vibrational Spectroscopy data for various Criegee intermediates. The numbers in parenthesis give the relative intensities of the bands as a percentage of the most intense band.

Criegee Intermediates	**Band Position (cm^{-1})**	**Description**	**References**
CH_2OO	v3 1434.1 v4 1285.9 v5 1213.3 v6 909.26 v8 847.44	CH_2 scissor/CO stretch CO stretch/CH_2 scissor OCH bend OO stretch/OCH_{trans} bend CH_2 wag	Huang et al. [96]
CD_2OO	v3 1318 v4 1054	CO stretch/CD_2 scissor OCD_{trans} bend/OO stretch	Huang et al. [96]

	v5 1017 v6 852	OCD_{cis} bend OO stretch/OCD_{trans} bend	
syn-CH_3CHOO	v4 1476.8 (30) v7 1280.8 (40) v8 1090.6 (10) v9 956.0 v10 871.2 (100)	CO stretch/HCO bend HCO bend/CO stretch CH_2 wag/CCH bend CCH bend/CH_2 wag OO stretch	Lin et al. [95]
anti-CH_3CHOO	v4 1479.0 (14) v7 1279.4 (17) v9 883.7 (100) v10 851.8 (73)	CO stretch/HCO bend HCO bend/CO stretch OO stretch CCH bend/CH_2 wag	Lin et al. [95]
$(CH_3)_2COO$	v7 1424 (45) v9 1368 (25) v11 1040 (20) v13 887.4 (100)	scissor of trans-CH_3 umbrella of cis-CH_3 CO stretch / CH_3 wag OO stretch	Wang et al. [97]

Microwave spectroscopic methods have also been used to detect various Criegee intermediates under molecular beam conditions. Nakajima and Endo [70] and McCarthy et al. [83] observed pure rotational transitions of CH_2OO and its isotopologues, cis-CHDOO, trans-CHDOO, CD_2OO, $CH_2{}^{18}OO$, $CH_2O{}^{18}O$, $CH_2{}^{18}O{}^{18}O$, $CD_2{}^{18}O{}^{18}O$, $^{13}CH_2OO$ using Fourier-transform microwave spectroscopy (FTMW). The assignments of the rotational transitions were confirmed by FTMW-mm wave double resonance spectroscopic methods. The CO bond length was found to be typical of a double bond and thus the ground state structure of the CH_2OO was verified to have dominant zwitterionic rather than biradical character. Twenty-four pure rotational transitions were observed for *anti*-CH_3CHOO by Nakajima et al. [101], and Nakajima and Endo [102] observed twenty-five transitions for *syn*-CH_3CHOO. The barrier for internal rotation of the methyl group was found to be substantially higher for the *syn*- conformer (837 cm^{-1}) compared with *anti*- conformer (399 cm^{-1}) suggesting strong interaction between one of the methyl hydrogen and terminal oxygen in the *syn*- conformer. A total of twenty-nine pure rotational transitions were observed for $(CH_3)_2COO$ [103]. The barrier heights for the internal rotation of the two methyl groups (733 and 543 cm^{-1}) were found to be similar to the *syn*- and *anti*- CH_3CHOO. The rotational constants for CH_2OO, CH_3CHOO (*syn*- and *anti*-conformers) $(CH_3)_2COO$, and CH_3CH_2CHOO (*syn1*-, *syn2*- and *anti*- conformers) were determined by fitting the transition frequencies using Watson's A-reduced Hamiltonian, and are listed in Table 5. Microwave spectroscopy has also been applied to characterize complexes and products from reactions of Criegee intermediates, as described in detail in the next section. Womack et al. [20] and Porterfield et al. [104] investigated the ozonolysis reaction of ethylene at atmospheric pressure and temperature in a fast-flow reactor, and detected the simplest Criegee CH_2OO along with other products ranging from pre-reactive complexes to secondary reaction products using microwave spectroscopy.

Table 5. Rotational constants for various Criegee intermediates. The uncertainties in the constants are given in parentheses.

Criegee Intermediates	Rotational constants (MHz)			References
	A	B	C	
CH_2OO	77748.8661(122) 77748.9491(186) 77752.655(16)	12465.2577(127) 12465.17311(175) 12465.247(13)	10721.2765(131) 10721.36435(161) 10721.313(16)	McCarthy et al. [83] Daly et al. [84] Nakajima and Endo [70]
syn-CH_3CHOO	17586.5295(15)	7133.4799(41)	5299.1704(40)	Nakajima and Endo [102]
anti-CH_3CHOO	48442.153(53)	4486.685(53)	4166.67037(50)	Nakajima et al. [101]
$(CH_3)_2COO$	8803.13851(94)	4328.49377(59)	3006.23840(57)	Nakajima and Endo [103]
syn1-CH_3CH_2CHOO	15827.30797(92)	2831.2119(12)	2474.3361(12)	Cabezas et al. [105]
syn2-CH_3CH_2CHOO	9165.3125(17)	3931.5104(62)	3178.4222(61)	Cabezas et al. [105]
anti-CH_3CH_2CHOO	14783.5573(16)	2870.62137(69)	2477.44947(53)	Cabezas et al. [105]

Berndt et al. [21] used chemical ionization mass spectrometry (CIMS) coupled with a free-jet flow system to detect Criegee intermediate adducts with protonated tetrahydrofuran and amines during ozonolysis of ethene and cyclohexene, with a detection limit of about 10^4 molecule cm^{-3}. The atmospheric pressure free-jet flow system allowed production and reaction of Criegee intermediates under wall free conditions before sampling by CIMS. The steady state concentrations of sampled Criegee intermediates at various concentration of co-reactants were used to estimate bimolecular reaction rate coefficients which were consistent with measurements from other direct methods using alkyl diiodide precursors. Giorio et al. [85, 106] used proton transfer reaction mass spectrometry to probe adducts formed from reactions of Criegee intermediates with the DMPO spin trap with a detection limit of around 10^9 molecule cm^{-3}. The Criegee intermediates were generated from ozonolysis of various biogenic and anthropogenic alkenes such as α-pinene, β-pinene, *cis*-2-hexene, methacrolein, styrene and limonene.

4. Reactivity of Criegee intermediates

The original sources of gaseous sCIs for laboratory studies were the ozonolysis of alkenes, with experiments conducted in reaction chambers used to deduce reaction rate coefficients. The development of more efficient and selective routes to sCI production, and hence direct spectroscopic detection (see the preceding section) has enabled direct measurement of sCI reaction kinetics, complementing the body of indirect measurements of sCI chemistry. Recent kinetic studies combined with computational calculations suggest that the Criegee intermediates can react rapidly, in many cases approaching or exceeding the classical gas-

kinetic limit, with closed shell species. Moreover, sCIs exhibit a range of different loss pathways including unimolecular decomposition, bimolecular reactions, and UV photolysis.

4.1 Unimolecular reactions

Criegee intermediates can thermally decompose via two main mechanisms: 1,3 ring closure forming a dioxirane type intermediate, or via transfer of hydrogen to the terminal oxygen forming a hydroperoxide [107]. The dioxirane mechanism is the main pathway for Criegee intermediates without α hydrogen atoms, such as CH_2OO. The dioxirane then decomposes to various products including OH via the 'hot acid channel' as shown for CH_2OO [44, 108]. In this process the sCI isomerizes through the dioxirane structure to form an energized carboxylic acid, followed by its decomposition to release OH and other products. The theoretical and experimental studies suggest a wide range of decomposition rate constants for different Criegee intermediates, which were briefly reported in our previous review (see Table 1 in Khan et al. [26]). From direct kinetic measurements using diiodomethane photolysis as a source, an upper limit (because of contributions of wall loss and side reactions) to the CH_2OO decomposition rate coefficient of 80-115 s^{-1} was deduced [63, 109]. A smaller upper limit to the decomposition rate coefficient of 11.7 s^{-1} estimated by Chhantyal-Pun et al. [66], is in better accord with the results of theoretical calculations giving a value of 0.3 s^{-1} [16, 110]. Berndt et al. [111] titrated CH_2OO from ethene ozonolysis with SO_2 to make H_2SO_4 and derived a rate coefficient of unimolecular reaction of CH_2OO of 0.19±0.07 s^{-1}. Most recently, Stone et al. [112] measured the first order removal of CH_2OO at elevated temperature, where the decomposition dominates. Their master equation model of the pressure and temperature dependence gave an extrapolated value of $1.1 \times 10^{-3} s^{-1}$ at 298 K and 760 Torr He. Decomposition yields of 63.7% for $H_2 + CO_2$, 36.0% for $H_2O + CO$ and 0.3% for OH + HCO were estimated from the master equation model.

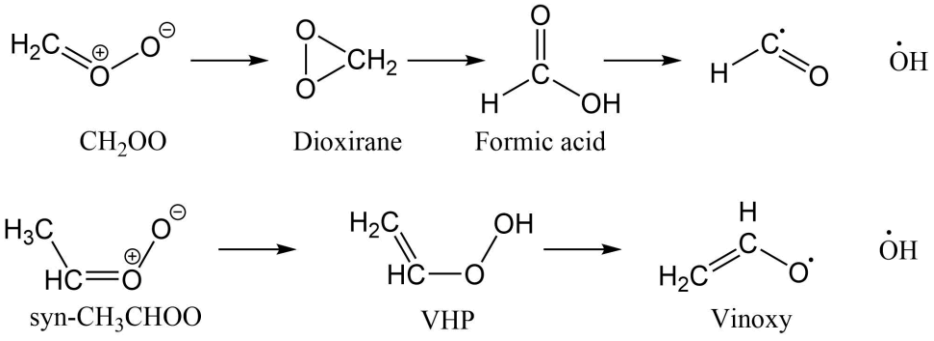

Scheme 2. Decomposition pathways of Criegee intermediates CH_2OO and *syn*-CH_3CHOO.

The decomposition of Criegee intermediates with α-hydrogen atoms, such as CH_3CHOO and $(CH_3)_2COO$, occurs via a 1,4 α-hydrogen transfer to the terminal oxygen atom forming a vinyl hydroperoxide (VHP) which in turn decomposes to yield OH and vinoxy radicals. Lester and co-workers have observed time resolved OH radical signals from unimolecular decomposition of CH_3CHOO, $(CH_3)_2COO$ and *syn*-MVKOO [82]. Only the *syn*-conformer of CH_3CHOO was observed to produce OH radical, whereas the *anti*-conformer decomposition is expected to follow a dioxirane pathway similar to CH_2OO. The interconversion barrier between the *syn*- and *anti*- conformers is predicted to be ~167 kJ mol^{-1} for CH_3CHOO and thus the two conformers act as separate species at atmospheric conditions. Taatjes et al. [113] observed production of hydroxyacetone from $(CH_3)_2COO$ decomposition and reaction pathway calculation suggested this was likely from migration of the OH group in the VHP intermediate. Unimolecular decomposition rate coefficients of 166, 369 and 33 s^{-1} at 298 K were estimated by Lester and co-workers for *syn*-CH_3CHOO, $(CH_3)_2COO$ and *syn*-MVKOO based on microcanonical rate coefficients measured under collision free conditions combined with master equation calculations [77, 114]. The details of these measurements and predictions are provided in a recent review [27]. Ambient measurements of the $(CH_3)_2COO$ unimolecular reaction rate coefficient by Smith et al. [115] and Chhantyal-Pun et al. [5] of 361±49 (298 K) and 305±70 s^{-1} (293 K) using UV absorption spectroscopy are in good agreement with the values calculated by Lester and co-workers. Indirect ozonolysis methods have also been used to measure unimolecular reaction rate coefficients, relative to reaction with scavengers such as SO_2 [43, 47, 49]. The unimolecular reaction rate coefficients derived from these ratios using known rate coefficients for reaction with SO_2 were shown to be in reasonable agreement with the directly measured values, albeit the derived values seem to consistently overestimate the unimolecular reaction rate [115]. Larger Criegee intermediates produced from ozonolysis of biogenic alkenes with double bonds are also predicted to undergo various ring closure and H transfer reactions, and unimolecular reactions are expected to be one of the dominant sinks in the troposphere [107]. Future studies of unimolecular reactions of larger Criegee intermediates using direct methods would therefore be enlightening on the importance of Criegee intermediates in the troposphere.

4.2 Insertion Reactions

Reagents such as alcohols, carboxylic acids and water have been used to trap and verify production of Criegee intermediates in condensed phase ozonolysis reactions [116] and the corresponding reactions have been extensively explored in the gas phase, as reviewed here.

Various computational studies have shown that Criegee intermediates react with organic and inorganic molecules containing polar covalent bonds with hydrogen as shown in Scheme 3 [68, 93, 110, 117-122]. These reactions are predicted to proceed by insertion of the Criegee intermediate into the polar bond. There are two main classes of insertion reactions: 1,4 insertion such as reactions with RCOOH and HNO_3, and 1,2 insertion such as reactions with HCl, H_2S, NH_3, ROH, ROOH and H_2O. The expected products of these reactions are multifunctional organic hydroperoxides, which can play an important role in secondary organic aerosol (SOA) formation in the troposphere.

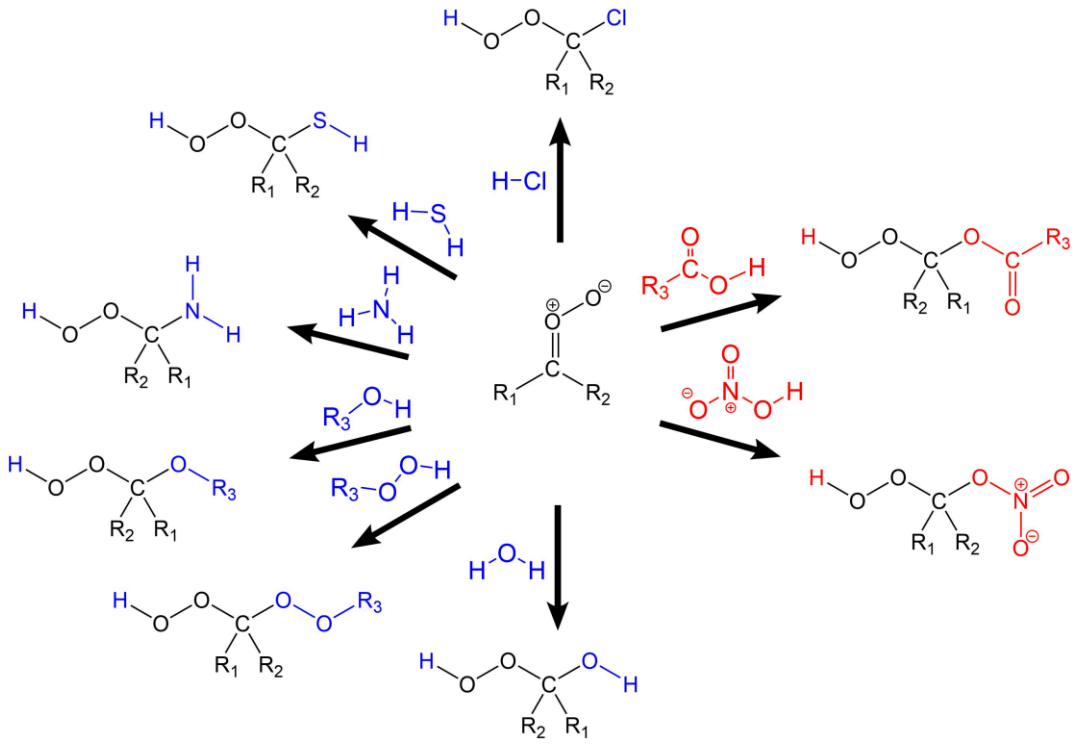

Scheme 3. 1,2 (blue) and 1,4 (red) insertion reactions of Criegee intermediates with various trace atmospheric molecules.

The kinetics of insertion reactions of Criegee intermediates have been measured by various research groups using direct methods such as multiplexed photoionization mass spectrometry (MPIMS) and UV absorption spectroscopy, and the resulting rate coefficient values are summarized in a previous review (see Table 2 and Table 6 in Khan et al. [26]). At ambient temperature, the rate coefficient ordering is H_2O < NH_3 ~ ROH < H_2S < HCl < RCOOH < HNO_3, ranging from about 2×10^{-16} cm^3 s^{-1} to 5×10^{-10} cm^3 s^{-1}. These reactions show weak dependence on pressure and negative dependence on temperature. Electronic structure calculations predict that these reactions proceed through formation of a pre-reactive complex, which then overcomes a cyclic transition state to produce functionalised organic

hydroperoxides as shown in Scheme 4 [68, 110, 118-122]. The 1,2 and 1,4 insertion reactions pass through 5-member and 7-member cyclic transition states, respectively. The 7-member cyclic transition state is submerged and nearly isoenergetic with the pre-reactive complex [68, 93, 117, 123]. The rate coefficients for the 1,4-insertion reactions are experimentally measured to be near to, or in some cases above the hard-sphere collision limit, and thus may be determined by long-range capture processes, in accord with theoretical predictions for barrierless reactions. The 5-member cyclic transition states are computed to range from near isoenergetic with the pre-reactive complex to above the reactant energy, consistent with experimentally measured 1,2 insertion reaction rate coefficients in the 10^{-11} to 10^{-16} cm^3 s^{-1} range.

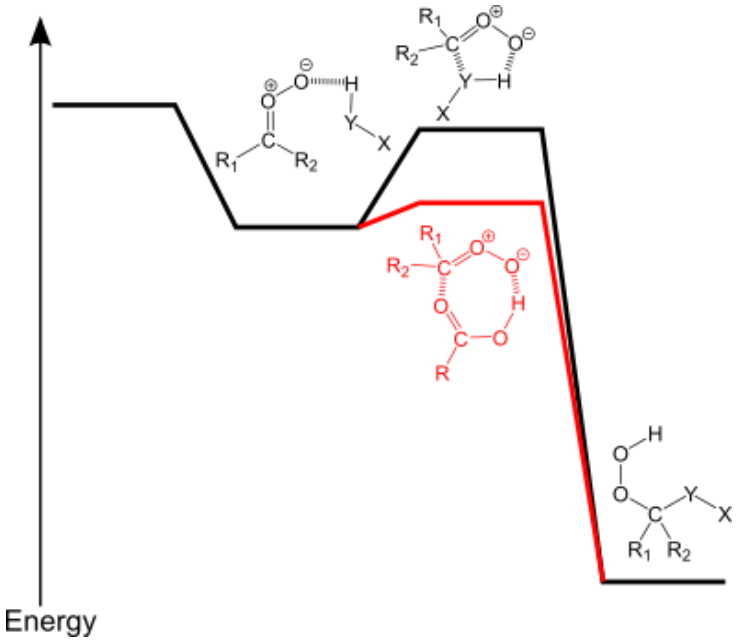

Scheme 4. Representation of the energy profiles along two alternative insertion reaction pathways of Criegee intermediates. The black and red lines show the reaction pathways for 1,2- and 1,4- insertion pathways, respectively. Structures of the reactants are provided in Scheme 3.

The rate coefficients for 1,4-insertion reactions of CH_2OO, *syn*-CH_3CHOO, *anti*-CH_3CHOO and $(CH_3)_2COO$ Criegee intermediates with various RCOOH were found by Chhantyal-Pun et al. [124] to correlate with the product of the dipole moments of the two reactants, as shown in Figure 5, supporting the idea that these rate coefficients are capture limited. A semi-empirical model based on dipole capture theory successfully describes the experimental rate coefficients reflecting the large dipole moments of the zwitterionic Criegee intermediates and the polarity

of the carboxylic acids. This model was applied to predict rate coefficients for reactions of atmospherically relevant, but difficult to measure, Criegee intermediates with RCOOH:

$$k = \mu^{-0.5}\left\{(1.9 \pm 0.2) \times 10^{-21}(\mu_{D1}\mu_{D2})^{\frac{2}{3}} - (6.3 \pm 0.7) \times 10^{-21}\right\} \quad \text{E1}$$

Here, $\mu_{D1}$and μ_{D2} are the dipole moments of the reactants in C•m and μ is the reduced mass of the reactants in kg. A fit to all the available experimental data returned an adjusted R^2 value of around 0.9 and thus equation (E1) provides a good structure activity relationship (SAR-Capture) for reactions of Criegee intermediates with carboxylic acids. The reactions of larger Criegee intermediates with RCOOH have also been predicted computationally to be barrierless, which supports the general applicability of the SAR-Capture model [93]. The gradient from the fit is in reasonable agreement with the value predicted for an isotropic capture suggested by dipole capture theory [125]. The negative intercept value in equation (E1) was postulated to reflect the failure of dipole-dipole capture theory in the limit of weak dipole-dipole attraction.

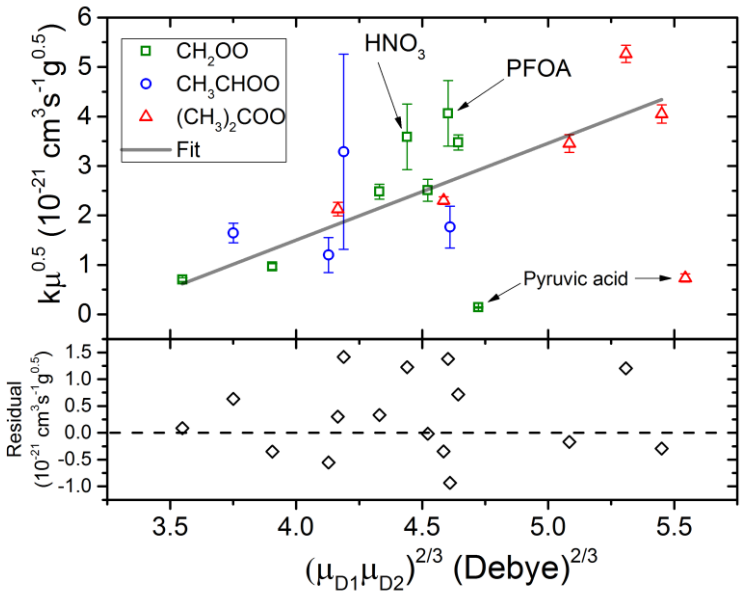

Figure 5. Structure−activity relationship based on a dipole−dipole capture model for the 1,4 insertion reaction rate coefficients of Criegee intermediates. The top panel shows experimental rate coefficients for CH_2OO (green squares), CH_3CHOO (blue circles), and $(CH_3)_2COO$ (red triangles) reactions with various carboxylic acids and HNO_3. The solid line is a linear regression based on the capture model including all the rate coefficients except the pyruvic acid data set. The bottom panel shows the residuals of the linear fit. Figure adapted (with addition of rate coefficients for reactions with perfluorooctanoic acid (PFOA) and HNO_3) from Reference [124] with permission from the American Chemical Society.

The recently measured rate coefficient value for reaction of CH_2OO with perfluoroacetic acid (PFOA) follows the trend predicted by the SAR-capture model, as shown in Figure 5 [126].

However, the rate coefficients for reaction of CH_2OO and $(CH_3)_2COO$ Criegee intermediates with pyruvic acid were significantly lower than those values expected from the SAR-Capture model. Pyruvic acid has a carbonyl group that can form an intramolecular hydrogen bond with the acidic hydrogen, which may hinder the 1,4-insertion reaction with a Criegee intermediate, resulting in a reduction in the rate coefficient. The rate coefficient for the reaction of CH_2OO Criegee intermediate with HNO_3 was also found to follow the SAR-Capture model, as shown in Figure 5, which supports a similar 1,4-insertion mechanism. Thus, the SAR-Capture model may be sufficiently robust to be used to predict rate coefficients for 1,4-insertion reactions of other Criegee intermediates with various RCOOH compounds and HNO_3. Predicted rate coefficient values from the SAR-Capture model are provided later. Further details of SAR prediction for rate coefficients of Criegee intermediates and carboxylic acids are reported in Chhantyal-Pun et al. [124] (see Table S3 of supplementary information). The rate coefficients of reactions with pinonic, terpinilic and nitric acids are relatively larger because of their larger dipole moments. Global modelling studies making use of the SAR-capture predictions have suggested that the fast 1,4-insertion reactions of Criegee intermediates are the dominant sink of carboxylic acids in the forested regions of the world [93, 124].

The reactions of Criegee intermediates CH_2OO and $(CH_3)_2COO$ with CF_3COOH show a negative temperature dependence [93]. The magnitude of the negative temperature dependence could not be described quantitatively by the dipole capture model. A reaction model based on branching between two pathways involving direct capture and stabilization of a pre-reactive complex, due to the presence of a low-lying transition state, was found to reproduce the observed temperature dependence. Thus, although the SAR-Capture model can describe the reactivity trends of the insertion reaction between Criegee intermediates and acids, a full quantitative description needs to consider the initial capture as well as entropic effects along the reaction pathway.

Murray and co-workers [68] correlated the rate coefficients of 1,2- and 1,4-insertion reactions for CH_2OO with the gas phase acidity of the co-reactants. They also showed that the rate coefficient values, plotted as a function of the labile hydrogen bond dissociation energy of the co-reactant, can be separated into two groups for the two insertion reactions. As an empirical observation, they reported that the rate coefficients for 1,2 insertion reactions were best correlated with the geometric mean of the bond dissociation energy and gas phase acidity. Tobias and Ziemann [127] also found that the relative rate coefficients of a C13 Criegee intermediate with heptanoic acid, formic acid, formaldehyde, 2-propanol and methanol are

correlated well with the gas phase acidity of the co-reactants. More recently, Chhantyal-Pun et al. [128] showed that the rate coefficients for 1,2 insertion reactions of CH_2OO with NH_3, H_2S, H_2O and CH_3OH are correlated significantly with the labile hydrogen bond dissociation energy (BDE) of the co-reactants. Figure 6 summarizes an updated set of directly measured rate coefficient values for the 1,2 insertion reactions. In this plot, the rate coefficient values for CH_2OO reactions with H_2O, NH_3, CH_3NH_2, CH_3OH, CH_3CH_2OH and $(CH_3)_2CHOH$ were found to be correlated well with BDE and a linear fit returns an R-square value of greater than 0.98.

$$k = (-0.126 \pm 0.008)\mathrm{BDE} + (26.9 \pm 3.8) \qquad \text{E2}$$

The linear fit expression, E2, predicts a rate coefficient value of 1.1×10^{-10} cm^3 $molecule^{-1}$ s^{-1} for the reaction of CH_2OO with $(CH_3)_2NH$. This trend of increasing reactivity of CH_2OO with increasing methyl substitution in amines is consistent with a recent computational study by Kumar and Francisco [129]. The rate coefficient for the CH_2OO + HCl reaction is larger than would be expected from the linear fit. The dipole moments for the 1,2 insertion reaction transition states are predicted to be significantly lower than the 1,4 reactions [130]. Therefore, the 1,2-insertion reactions likely proceed by homolytic not heterolytic cleavage of the labile bond to hydrogen. However, the dipole moment of the CH_2OO + HCl reaction transition state is of similar magnitude to that of the 1,4- insertion reaction transition states, suggesting a degree of heterolytic cleavage character which may explain the relatively large rate coefficient. The rate coefficient values for CH_2OO reactions with CH_3SH and H_2S were found to be smaller than expected from the linear fit of equation E2, as shown in Figure 6. This is likely because the attractive forces between the Criegee intermediate carbonyl carbon and sulphur (a third-row element) are not as strong as with oxygen and nitrogen (second-row elements). However, the rate of increase in rate coefficient is similar for both group of reactants. The reaction of CH_2OO with $(CH_3)_2S$ was found to be slow, likely because of the absence of labile hydrogen atoms, and only an upper limit value of $< 1 \times 10^{-14}$ cm^3 $molecule^{-1}$ s^{-1} could be estimated [131].

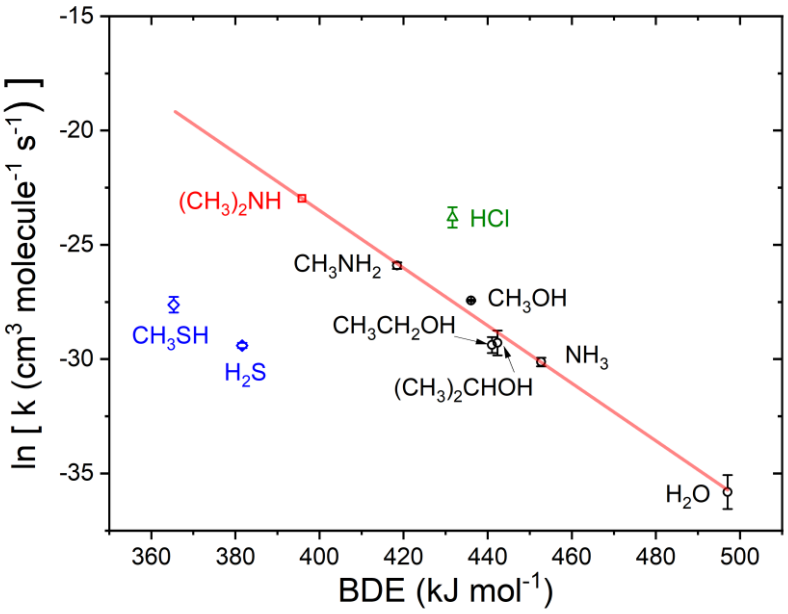

Figure 6. Comparison of the rate coefficients for various 1,2-insertion reactions of CH_2OO Criegee intermediates with the bond dissociation energy of the labile hydrogen atom. The bond dissociation energies were obtained from the CRC Handbook [132]. The solid line is a linear fit to the rate coefficient values for reaction with CH_3NH_2 [128], CH_3OH [94, 130], CH_3CH_2OH [94, 130], $(CH_3)_2CHOH$ [130], NH_3 [128, 133] and H_2O [92, 111]. The rate coefficient values for reaction with HCl [68], H_2S [131, 134] and CH_3SH [131, 135] are also shown. In case of rate coefficient with multiple measurements, an averaged value was taken as the best estimate.

The reactions of $(CH_3)_2COO$ with NH_3 [128] and H_2O [75] are significantly slower compared with that of CH_2OO. Consistent with these observations, the barrier heights for the transition states of these reactions are predicted to be above the reactant energy for $(CH_3)_2COO$ and submerged for CH_2OO [110, 119]. Sheps et al. [72] observed that the 1,2-insertion reaction of *anti*-CH_3CHOO with H_2O is significantly faster than the reaction of *syn*-CH_3CHOO, consistent with barrier height calculations of Long et al. [110]. Similarly, laboratory and computational studies of Chao et al.[136] found reaction of CH_3OH with *anti*-CH_3CHOO to be significantly faster than with syn-CH_3CHOO. The reaction of *syn*-CH_3CHOO with H_2O [110] and $(CH_3)_2COO$ with CH_3OH [137] have been predicted to be significantly enhanced by hydrogen atom tunnelling. However, because of limited experimental datasets, it is hard to empirically identify general trends in 1,2-insertion reactions resulting from changes in the structure of the Criegee intermediate.

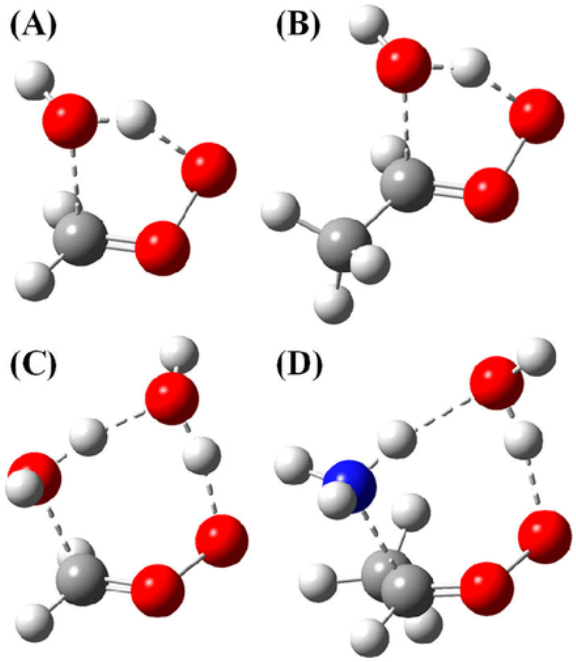

Figure 7. Schematic geometries of transition states for $CH_2OO + H_2O$ (A), anti-$CH_3CHOO + H_2O$ (B), syn-$CH_3CHOO + (H_2O)_2$ (C) and syn-$CH_3CHOO + NH_3 + H_2O$ (D) reactions. Figure reprinted from Reference [136] with permission from the American Chemical Society.

The rate coefficients for some of the 1,2-insertion reactions of Criegee intermediates have been shown to be catalysed by the presence of a water molecule. For example, reaction of CH_2OO with H_2O is enhanced by a factor of 3000 by a second H_2O molecule [92]. Similarly, reaction with methanol is nearly 3 times faster with an extra water molecule [138]. Quantum chemistry calculations predict the formation of a submerged seven-member cyclic transition state incorporating the additional water molecule for reactions of CH_2OO, *syn*-CH_3CHOO, *anti*-CH_3CHOO and $(CH_3)_2COO$ with H_2O, as shown in Figure 7 [136, 138-140]. The seven-member cyclic transition state, as is found for the 1,4-insertion reactions of Criegee intermediates, is significantly more stable than the five-membered cyclic transition state arising in the absence of a water molecule, which accounts for the enhancement of the reaction rate coefficient. Similar enhancements are expected for other 1,2-insertion reactions of Criegee intermediates. The reactions with water monomer/dimer along with unimolecular reactions are the dominant sinks for most Criegee intermediates in the troposphere [26, 94, 107]. However, the 1,4-insertion reactions are fast and could compete with these dominant sinks under certain conditions, whereas the 1,2-insertion reactions, even with enhancement in the presence of a water molecule, are in general too slow to compete in the troposphere with reaction with water vapour or unimolecular decomposition.

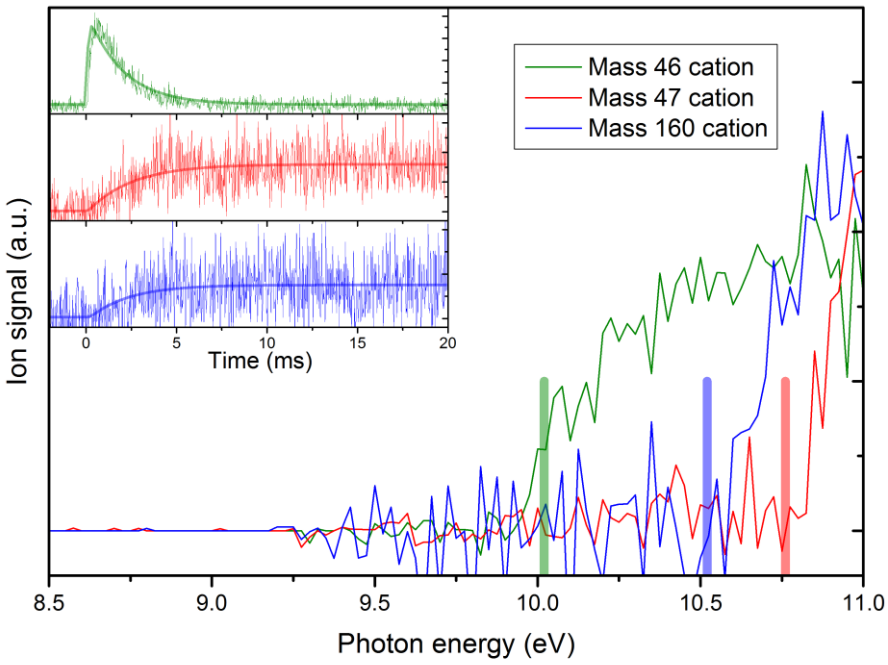

Figure 8. Observation of a MFOHP from the insertion reaction of CH_2OO with CF_3COOH using multiplexed photoionization mass spectrometry. The solid lines are photoionization spectra of different mass cations observed after initiation of the reaction. The vertical bars show predicted appearance energies of CH_2OO^+ (mass 46), CH_2OOH^+ (mass 47), and $CF_3COOCH_2OOH^+$ (mass 160). The inset displays kinetic traces of the m/z 46, 47, and 160 species. Figure reprinted from Reference [124] with permission from the American Chemical Society.

The insertion reactions of Criegee intermediates have been predicted to produce multifunctional organic hydroperoxides (MFOHPs), as shown in Scheme 3. Direct observation of MFOHPs has proven possible using MPIMS [124, 128]. The MPIMS method probes both the time and photon energy-dependent ionization profiles of various species involved in a chemical reaction, which allows detailed structural and kinetic characterizations of these species [141]. The MFOHPs produced from the 1,4-insertion reaction of CH_2OO with CF_3COOH (shown in Figure 8) and $(H_2O)_2$ have been shown to ionize to a stable cationic state [92, 124]. Other MFOHP products of reactions of CH_2OO and RCOOH undergo dissociative ionization in the cationic state to produce CH_2OOH^+ (mass 47 in Figure 8) and co-fragments, confirmed using quantum chemistry calculations along the intrinsic reaction coordinate [124]. The appearance energy for the dissociative ionization process was calculated by subtracting the ground state energy of the neutral molecule from the energy of the transition state of the dissociation channel in the cationic state. Similarly, the MFOHP formed from the 1,2-insertion reaction of CH_2OO with CH_3NH_2 undergoes dissociative ionization to $CH_3N(H)CH_2^+ + HO_2$ and $CH_3N(H)CHO^+ + H_2O$ [128]. The dissociative ionization pathways in the MFOHP cationic states were also confirmed using intrinsic reaction coordinate and appearance energy

calculations. Using MPIMS, Sheps et al. [92] observed hydroxymethyl hydroperoxide, one of the simplest MFOHP, to be one of the major products from the reaction of CH_2OO with $(H_2O)_2$.

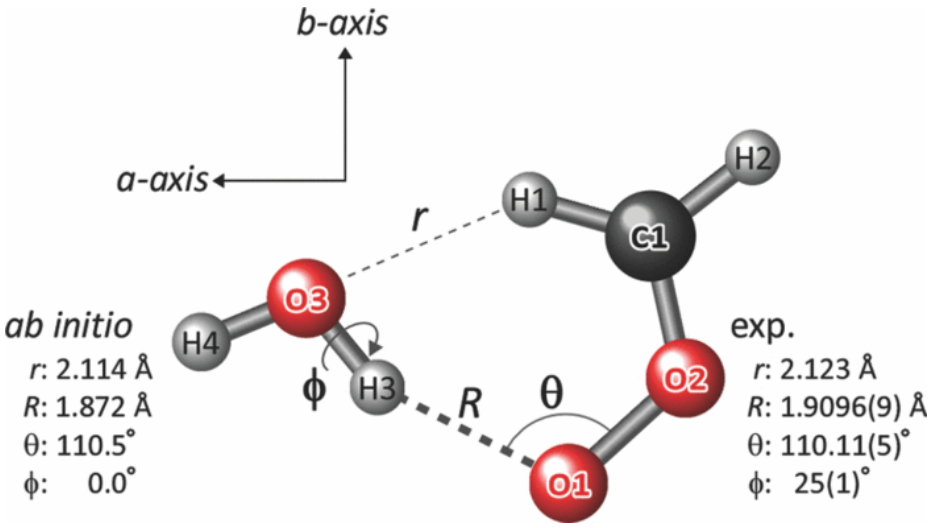

Figure 9. Geometry of the pre-reactive complex involved in the $CH_2OO + H_2O$ reaction, obtained using Fourier Transform Microwave Spectroscopy. The ab initio calculations were performed at the CCSD(T)/aug-cc-pVTZ level of theory. Figure reprinted from Reference [142] with permission from AIP Publishing.

MFOHPs from reaction of CH_2OO with HCOOH, CH_3COOH and CH_3OH have been observed in static chamber studies using Fourier transform infrared spectroscopy by Neeb et al. [35]. Recently, Chung et al. [69] observed formation of hydroperoxymethyl formate (HPMF) from the CH_2OO + HCOOH reaction using time resolved step scan infrared spectroscopy. They were also able to observe decomposition of one of the HPMF conformers to formic acid anhydride, consistent with previous static chamber studies. Endo and co-workers have observed MFOHP products from CH_2OO + HCl [143], CH_2OO + HCOOH [144] and $CH_2OO + H_2O/(H_2O)_2$ [101] reactions using Fourier transform microwave spectroscopy. They were also able to observe pre-reactive complex formation in the $CH_2OO + H_2O/(H_2O)_2$ reaction system [142], as shown in Figure 9, but not in the CH_2OO + HCl [143] and CH_2OO + HCOOH reaction systems [144]. This indicates that the pre-reactive complex in the latter two reactions promptly reacts, in agreement with low reaction barrier predicted by theoretical calculations [68, 117, 143]. No systematic experiments have been performed for yield measurement of MFOHPs at ambient conditions from the insertion reactions. Liu et al. [145] have also observed evidence for catalytic isomerization of Criegee intermediates with α-hydrogens to vinyl hydroperoxides, in the presence of formic and acetic acids. Ab initio and master equation studies by Vereecken et al. [117] and Raghunath et al. [146] predict that most of the hydroperoxide adducts produced from CH_2OO reactions with HCOOH and HNO_3, respectively, are stabilized at ambient conditions.

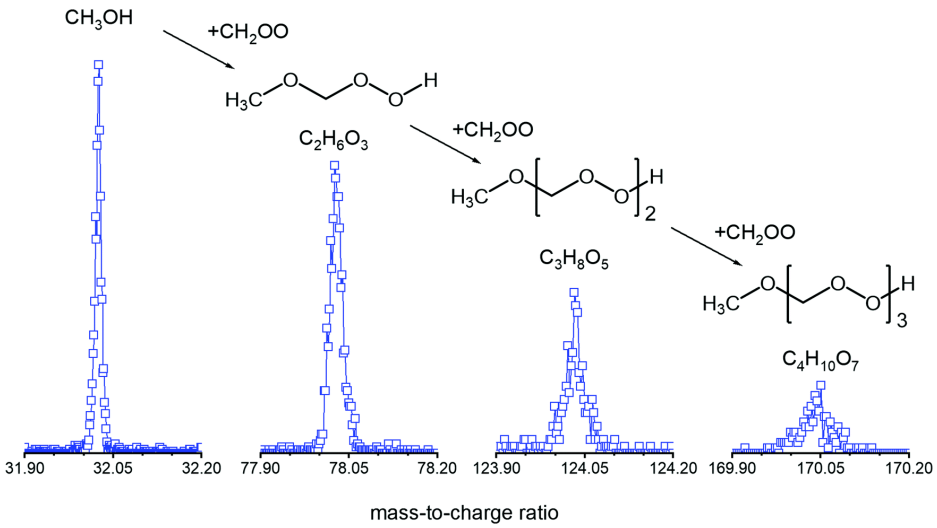

Figure 10. Mass spectra of sample products from a jet stirred reactor during ozonolysis of ethene. The masses of the cations are consistent with sequential addition reactions of Criegee intermediate CH_2OO with CH_3OH. Figure reprinted from Reference [147] with permission from the PCCP Owner Societies.

No direct observations have been reported for the reaction of Criegee intermediates with hydroperoxides. However, Hansen and co-workers recently observed oligomers from sequential addition of CH_2OO with H_2O, HCOOH, CH_3OH, C_2H_5OH, H_2O_2, CH_3OOH, C_2H_5OOH, CH_3CHO, $HOCH_2CHO$, $HOOCH_2CHO$ and C_2H_4 during ozonolysis of ethene in a jet stirred reactor as shown in Figure 10 for the reaction with CH_3OH [147]. The addition products were measured using energy resolved photo-ionization mass spectrometry with the aid of quantum chemistry calculation. The observed appearance energies of various cations were in good agreement with the calculated appearance energies for hydroperoxides with CH_2OO units. The reactions were postulated to proceed by 1,2 insertion of CH_2OO with various reactants produced from the ozonolysis to form a hydroperoxide. These hydroperoxides can then react further with CH_2OO through the 1,2-insertion mechanism as shown in Scheme 4 to form adduct hydroperoxides. Sakamoto et al. [148] also observed oligomeric organic hydroperoxides with CH_2OO chain units, likely from sequential insertion of CH_2OO to a hydroperoxide, using negative ion chemical ionization mass spectrometry of gas and particle phase product samples from ethylene ozonolysis experiments carried out in a Teflon bag reactor. Vereecken et al. [122] predicted a reaction pathway leading to formation of a pre-reactive complex and then to a hydroperoxide adduct, similar to the pathways shown in Scheme 4. However, the minimum energy pathway is predicted to form ether oxides in the case of CH_2OO + CH_3OOH and $(CH_3)_2COO$ + CH_3OOH reactions.

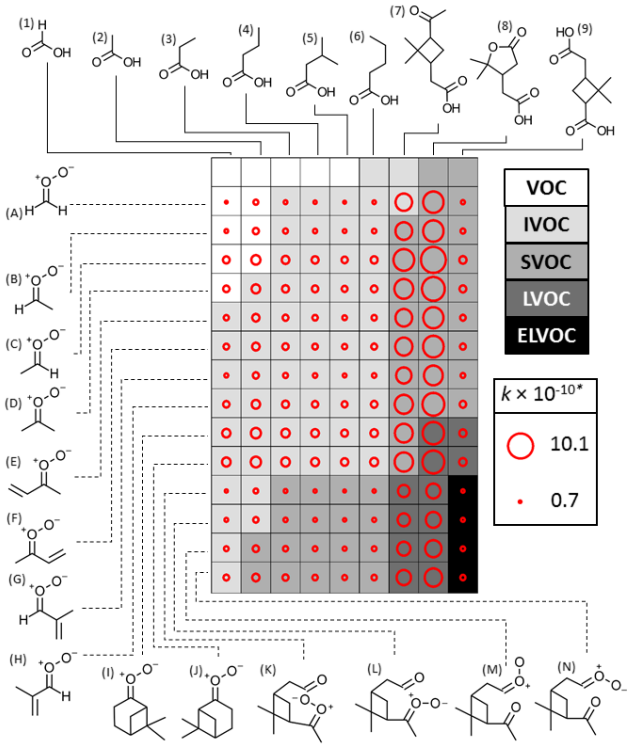

Figure 11. Volatilities of the adduct products from the Criegee intermediate + carboxylic acid reactions. Volatilities are shown in grey shading and the labels IVOC, SVOC, LVOC, and ELVOC stand for intermediate, semi, low, and extremely low volatile organic compound, respectively. The saturation concentration ranges for these classifications are provided in Donahue et al. [149]. The diameter of each red circle indicates the magnitude of the predicted rate coefficient (*units of cm^3 s^{-1}) estimated from the SAR of Equation (E1). Figure reprinted from Reference [124] with permission from the American Chemical Society.

Figure 11 shows the predicted vapour pressures of various MFOHPs, obtained from Criegee intermediate + carboxylic acids reactions, using an empirical model based on the group contribution technique [150, 151]. The inputs to the model are described by Chhantyal-Pun et al. [124] and the volatility classification are those used by Donahue et al. [149]. MFOHPs produced from reaction of Criegee intermediates derived from pinene ozonolysis with large biogenic carboxylic acids, such as pinonic acid, pinic acid and terpenylic acid, are predicted to have low to extremely low volatility, and are therefore likely to condense to form SOA as shown in Scheme 5.

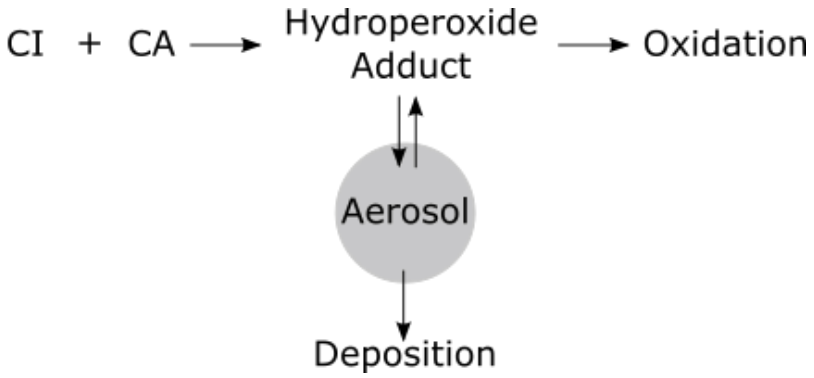

Scheme 5. Schematic pathway of a Criegee intermediate (CI) insertion reaction (with carboxylic acid, CA) leading to formation of secondary organic aerosol.

The fast rate coefficients for production of low volatility MFOHPs suggest that the 1,4-insertion reactions will be an important source of SOA in forested regions around the globe. Figure 12 shows the result of a global atmospheric model simulation performed by Chhantyal-Pun et al. [124] which predicts an increase in SOA concentrations of up to 0.89 μg m^{-3} resulting from reaction of Criegee intermediates with pinonic acid, compared with global average SOA concentration of 2.8 μg m^{-3} [152]. The SOA contribution from Criegee intermediate chemistry is dependent on the estimate of steady state concentrations of Criegee intermediates in the troposphere which are being actively refined using new experimental as well as computational efforts. Studies by Enami and Colussi have further shown that Criegee intermediates can react efficiently with alcohols and carboxylic acids at the air water interface and thus may facilitate particle growth [153, 154].

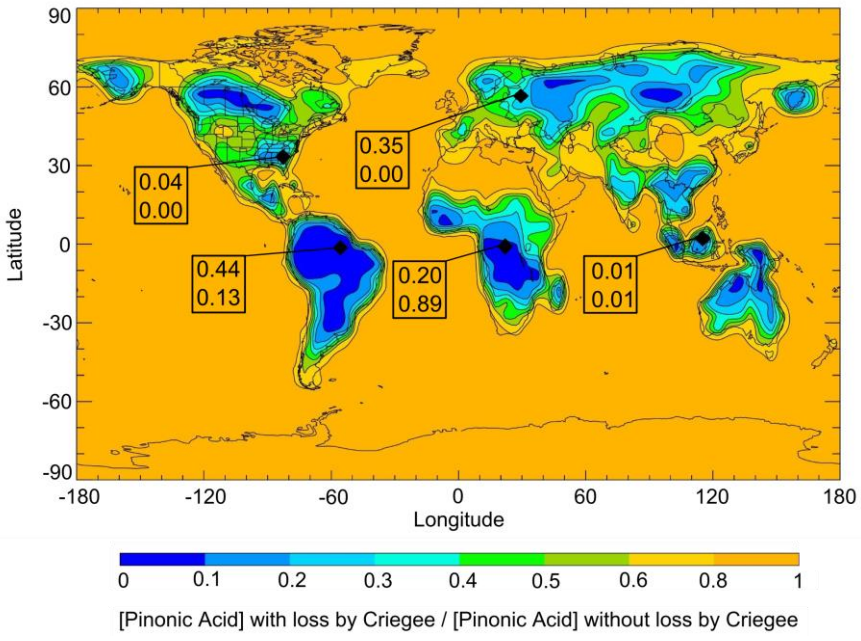

Figure 12. Reduction of Pinonic acid after inclusion of reaction with Criegee intermediates predicted using the STOCHEM-CRI model. The numbers in the boxes represent average SOA concentrations (in μg m^{-3}) during

summer (June, July, August, top) and winter (December, January, February, bottom) at various places indicated by the diamond symbols. Figure reprinted from Reference [124] with permission from the American Chemical Society.

4.3 Cycloaddition Reactions

Criegee intermediates are expected to undergo cycloaddition reactions as is typical for 1,3 dipoles [116]. Computational studies have predicted addition of Criegee intermediates across double bonds of various molecules such as carbonyls [155], alkenes [91, 156] and SO_2 [157, 158], as shown in Scheme 6. Criegee intermediates are also predicted to self-react to form six-membered cyclic biperoxides as shown in Scheme 6 [156]. These additional chemicals are present in ozonolysis experiments either as a source or scavenger of Criegee intermediates or as a side product. Thus, characterisations of these reactions are important in understanding the ozonolysis studies. The cyclic ozonide produced from reaction with SO_2 can decompose to form SO_3 which is a primary precursor to H_2SO_4, itself an important precursor for nucleation and aerosol formation in the atmosphere.

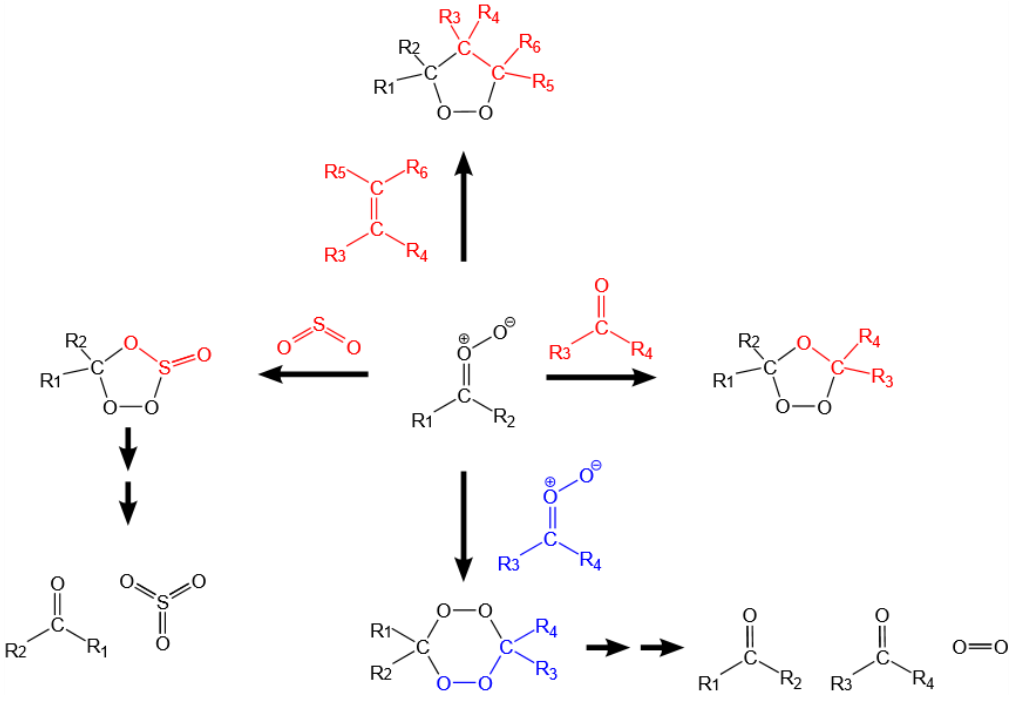

Scheme 6. Cycloaddition reactions of Criegee intermediates with various molecules.

Rates of reaction of the CH_2OO Criegee intermediate with CH_3CHO, CH_3COCH_3 and CF_3COCF_3 have been measured using photoionization spectrometry and UV absorption spectroscopy [4, 159, 160] and the rate coefficients were found to increase in the order CH_3COCH_3 < CH_3CHO < CF_3COCF_3 (see Table 6 in Khan et al. [26]). The reactions of Criegee intermediates with carbonyl compounds and alkenes are predicted to form pre-reactive

complexes and then proceed over a transition state to form a heteroozonide (secondary ozonide), similar to the pathway shown in scheme 4 for insertion reactions [155, 159]. The experimental observations are consistent with quantum chemistry calculations that predict that the transition state is stabilized more effectively in the presence of electron withdrawing substituent groups in the carbonyl compound. The reactions of CH_2OO with CH_3COCH_3 and CH_3CHO were recently found by Elsamra et al. [159] to have weak pressure and negative temperature dependences in the 298 to 500 K range, consistent with small re-dissociation of reaction intermediates back to reactants and a submerged barrier. Chhantyal-Pun et al. [161] further studied the CH_2OO reaction with CH_3COCH_3 at atmospherically relevant conditions and found that the rate coefficient increases by a factor of 5 going from a temperature of 310 to 250 K, as shown in Figure 13. Products were observed at the adduct masses for the CH_2OO reactions with CH_3COCH_3 and CF_3COCF_3, at 4 Torr (He) and 293 K, and the appearance energies were consistent with photoionization of a secondary ozonide product, as shown in Scheme 6 [4, 159]. The yield of secondary ozonide is expected to increase further at higher pressure because of increased collisional stabilization. Chamber experiments by Neeb et al. also showed formation of secondary ozonides during ozonolysis of ethene in the presence of acetaldehyde and acetone at 730 Torr (synthetic air) and 296 K [36]. These authors observed production of HCOOH and HCHO, which are predicted to be dissociation products of the secondary ozonide, thus resulting in catalytic isomerization of CH_2OO. Rate coefficients of reactions of CH_2OO with various alkenes like ethene, propene, isobutene, 1-butene and 2-butene were measured to be around 1×10^{-15} cm^3 s^{-1}, significantly smaller than reactions with carbonyls [91]. The reactions with alkenes exhibit a weak positive temperature dependence in the 298 to 494 K range [91], consistent with predicted higher energy transition states (isoenergic to the energy of separated reactants) for the cyclo-addition reactions with alkenes compared with carbonyls [155, 156].

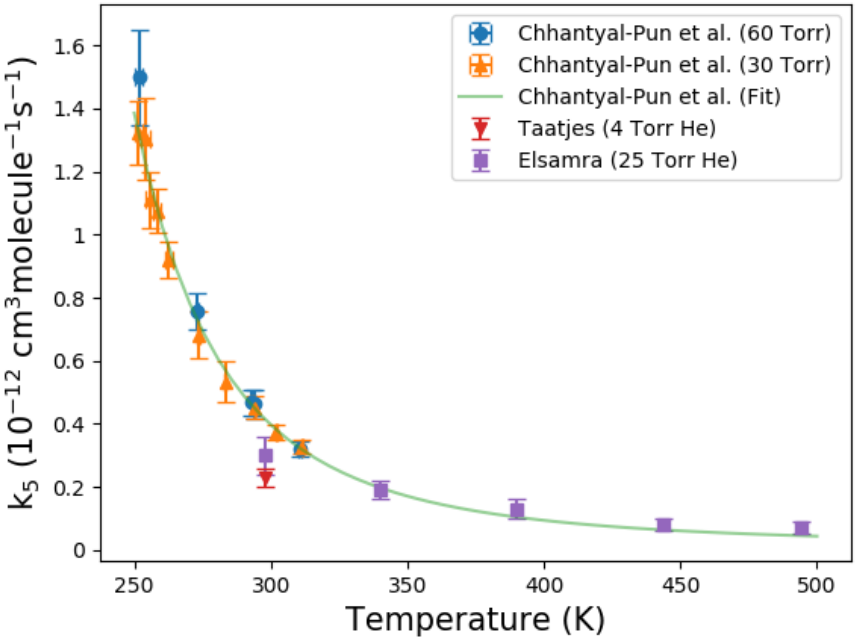

Figure 13. Temperature dependence of the reaction of CH_2OO with CH_3COCH_3. The blue circle and orange triangle datapoints are obtained from studies of Chhantyal-Pun et al. [161] The scarlet triangle and violet square datapoints are taken from studies of Taatjes et al. [4] and Elsamra et al. [159] respectively. The solid green line shows a semi-empirical analytical fit the dataset. Figure adapted from Reference [161] with permission from the American Chemical Society.

The rate of self-reaction of the CH_2OO Criegee intermediate has been measured by Buras et al. [67], Chhantyal-Pun et al. [66] and Ting et al. [162] using UV absorption spectroscopy. The derived rate coefficient (see Table 6 in Khan et al. [26]) is near the hard-sphere collision limit (~ 7×10^{-11} cm^3 s^{-1}). Furthermore, Chhantyal-Pun et al. [5] measured a self-reaction rate coefficient for $(CH_3)_2COO$ of 6×10^{-10} cm^3 s^{-1}, which is greater than the hard-sphere collision limit but within the dipole capture limit. The $(CH_3)_2COO$ Criegee intermediate is predicted to have a dipole moment of 5.48 D, compared with 4.31 D for CH_2OO, implying greater dipole-dipole attraction and a higher self-reaction rate coefficient. However, the observed difference in the self-reaction rate coefficient is larger than that predicted by the dipole capture theory. A computational study by Vereecken et al. predicted a barrierless CH_2OO self-reaction with an excess energy of around 400 kJ mol^{-1} for the formation of the cyclic biperoxide as shown in Scheme 7 [157]. The cyclic biperoxide is predicted to undergo sequential homolytic cleavage of the peroxide bond to form oxygen and two carbonyl molecules. Similar reaction pathways can be expected for the $(CH_3)_2COO$ self-reaction. The self-reaction rate coefficient of $(CH_3)_2COO$ was also found to be independent of temperature in the range 250 to 310 K, consistent with a negligible barrier to reaction, and with a rate coefficient limited by dipole-

dipole attraction [93]. Several studies have observed production of carbonyl compounds during reactions of CH_2OO and CH_3CHOO, using MPIMS or laser induced fluorescence detection, possibly because of self-reaction [2, 75, 160].

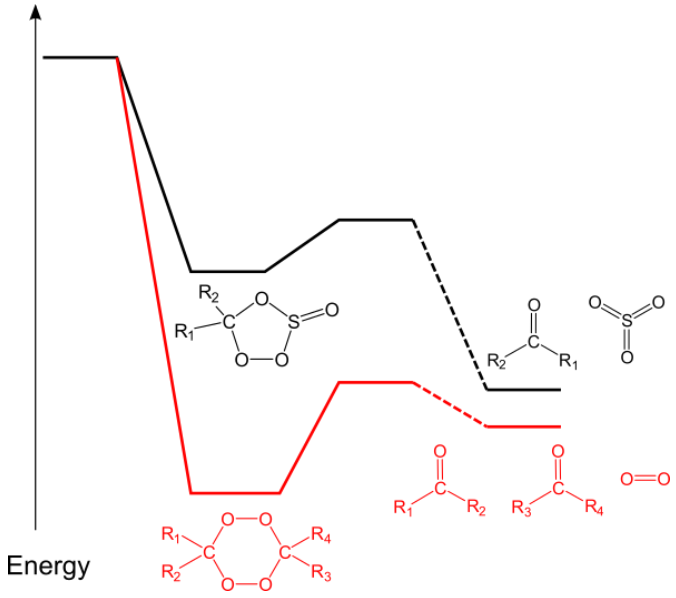

Scheme 7. Representation of the potential energy along the reaction coordinate for the cycloaddition reaction of a Criegee intermediate with itself (red) and with SO_2 (black). Structures of the reactants are provided in Scheme 6.

The reactions of CH_2OO, *syn*-CH_3CHOO, *anti*-CH_3CHOO and $(CH_3)_2COO$ Criegee intermediates with SO_2 have been probed directly using multiplexed photoionization spectrometry [2, 5, 19] and UV absorption spectroscopy methods [66, 72, 75, 90]. The rate coefficients for CH_2OO/*syn*-CH_3CHOO and *anti*-CH_3CHOO/$(CH_3)_2COO$ were found to be similar (see Table 5 in Khan et al. [26]), suggesting comparable reaction pathways. Similar to the cyclo-addition reactions of Criegee intermediates with alkenes and carbonyls, the reactions of Criegee intermediates with SO_2 have been predicted to proceed by formation of a pre-reactive complex before crossing a submerged barrier to form an ozonide structure as shown in Scheme 7 [157, 158]. The submerged barrier is consistent with experimental observations of large rate coefficients. The Criegee intermediates with larger dipole moments (5.53 D for *anti*-CH_3CHOO and 5.48 D for $(CH_3)_2COO$) have about an order of magnitude larger rate coefficients for SO_2 reaction than Criegee intermediates with lower dipole moments (4.69 D for *syn*-CH_3CHOO and 4.31 D for CH_2OO) [19, 72], suggesting a role for long-range interactions in the reaction rate coefficients [5]. The dipole moments of larger Criegee intermediates, derived from ozonolysis of biogenic hydrocarbons, are predicted to be greater than for CH_2OO. Therefore, rate coefficients in the 10^{-11} to 10^{-10} cm^3 s^{-1} range can be expected

for the reactions between Criegee intermediate and SO_2, based on the laboratory observations so far.

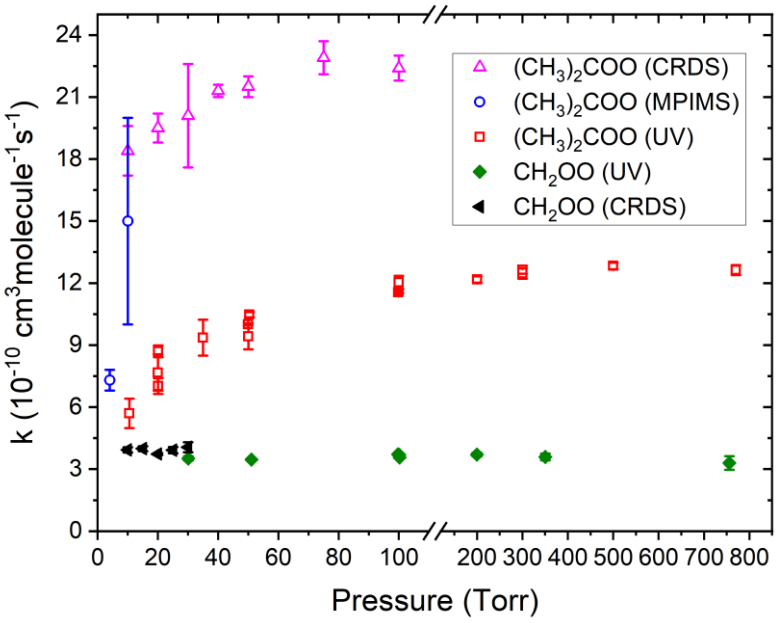

Figure 14. Pressure dependence of reaction of $(CH_3)_2COO$ Criegee intermediate with SO_2 at room temperature. The CRDS dataset for CH_2OO was obtained from Chhantyal-Pun et al. [66]. The CRDS and MPIMS dataset for $(CH_3)_2COO$ were obtained from Chhantyal-Pun et al. [5]. The UV datasets for CH_2OO and $(CH_3)_2COO$ were obtained from Huang et al. [75].

The rate coefficient for the reaction between CH_2OO and SO_2 is independent of pressure [66, 75], as shown in Figure 14, indicating little re-dissociation of the ozonide to reactants, and at low pressure (4 Torr He) this reaction was shown using MPIMS to produce SO_3 [19]. Using time resolved step-scan infrared spectroscopy, Wang et al. [163] observed formation of SO_3 and HCHO from reaction of CH_2OO with SO_2 at pressure of 110 Torr. These observations are consistent with predicted decomposition of the initial secondary ozonide to SO_3 and HCHO as shown in Scheme 7 [157, 158]. The rate coefficient for the $(CH_3)_2COO$ + SO_2 reaction has a positive pressure dependence, suggesting some stabilization of an association reaction intermediate and non-negligible dissociation back to reactants. Using CRDS and MPIMS, Chhantyal-Pun et al. [5] measured a relatively small pressure dependence, with rate coefficients increasing by 20 percent, compared to an increase of 100 percent measured by Huang et al. [75] in the 10 to 100 Torr range as shown in Figure 14. A weak negative temperature dependence was reported by Smith et al. [115] for the $(CH_3)_2COO$ + SO_2 reaction in the 283 to 323 K range. Computational studies by Kuwata et al. [158] estimate a 96.2% yield for prompt carbonyl and SO_3 formation, whereas Vereecken and co-workers [157] estimate > 97% collisional stabilization of the cyclic secondary ozonide. Kuwata and co-workers suggest that

the reaction proceeds mainly through a closed-shell pathway resulting in simultaneous cleavage of the O-O and CO bonds to form SO_3 and $(CH_3)_2CO$. Instead, Vereecken and co-workers suggest that the reaction proceeds through an open-shell pathway resulting in sequential cleavage of O-O and CO bonds to form a diradical intermediate before forming SO_3 and $(CH_3)_2CO$. Chhantyal-Pun et al. [5] also showed evidence for catalytic isomerization of $(CH_3)_2COO$ in the presence of SO_2 and the isomerization product signal was consistent with a combination of 2-hydroperoxypropene and methyldioxirane. Kuwata et al. [158] estimated a 2.5% yield for isomerization of $(CH_3)_2COO$ to the $CH_3C(O)OCH_3$ ester, in the presence of SO_2, which may also contribute to the observed isomerization signal.

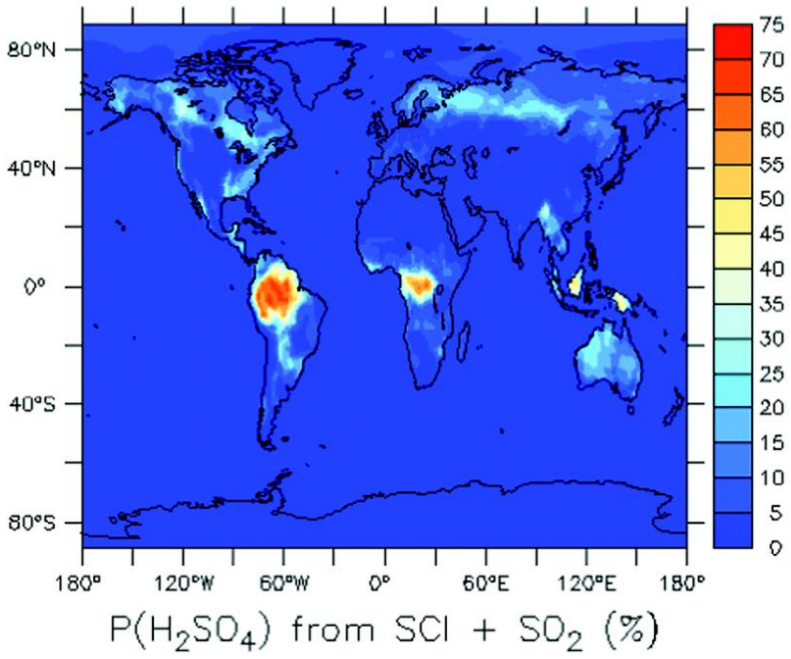

Figure 15. Modelled annual percent contribution of Criegee intermediates reaction with SO_2 to production of tropospheric H_2SO_4. The only other H_2SO_4 source considered is reaction of OH + SO_2. Figure adapted from Reference [107] with permission from the PCCP Owner Societies.

Atmospheric reaction of SO_3 with water forms sulfuric acid which is an important precursor to aerosol formation [164]. Figure 15 shows that Criegee intermediate reaction with SO_2 is estimated to contribute up to ~70% of H_2SO_4 production in the Amazon region. The reactions of larger atmospherically relevant Criegee intermediates with SO_2 may involve greater collisional stabilization of secondary ozonide intermediates because of the greater number of degrees of freedom. However, an ozonolysis flow tube study by Sipilä et al. [53] coupled with detection of sulfuric acid suggested that even for larger Criegee intermediates produced from the ozonolysis of isoprene, α-pinene and limonene, the yield of SO_3 from reaction with SO_2 might be close to unity. Direct yield studies of SO_3, as well as the chemistry and structures of

the reaction intermediates, need to be pursued to quantify better the importance of these reactions in the troposphere.

4.4 Addition Reactions

Criegee intermediates can react with various trace molecules in the troposphere which possess unpaired electrons, including NO, NO_2 and RO_2 radicals. Direct MPIMS studies have shown that the reaction of CH_2OO with NO is slow, with a rate coefficient $< 6 \times 10^{-14}$ cm^3 s^{-1} [2], consistent with predictions of a high energy barrier [157]. In contrast, reactions of sCIs (C1-C3) with NO_2 have bimolecular rate coefficients in the range of $\sim 10^{-12}$ cm^3 s^{-1} [2, 5, 19]. The rate coefficient for reaction of CH_2OO with NO_2 has been refined by Stone et al. [160] to be $(1.5\pm0.5)\times10^{-12}$ cm^3 $molecule^{-1}$ s^{-1} using laser induced fluorescence of HCHO, as a proxy for CH_2OO, and Luo et al. [100] to $(1.0\pm0.2)\times10^{-12}$ cm^3 $molecule^{-1}$ s^{-1} using quantum cascade laser infrared spectroscopy of CH_2OO. A computational study by Vereecken and co-workers showed that the minimum energy pathway for the NO_2 reaction involves a pre-reactive complex and nitroalkyl peroxy radical product, connected by a submerged barrier [165]. The competing reaction pathway leading to formation of NO_3 was predicted to have a high barrier and is thus not accessible under ambient conditions. Both predictions are consistent with observation of only adduct product formation by direct studies [166]. These outcomes suggest that the previous observation of NO_3 in indirect studies may have resulted from side reactions of species generated during the reaction initiation step [167]. Chhantyal-Pun et al. [5] also showed evidence for isomerization of $(CH_3)_2COO$ to 2-hydroxypropene and methyldioxirane in the presence of NO_2.

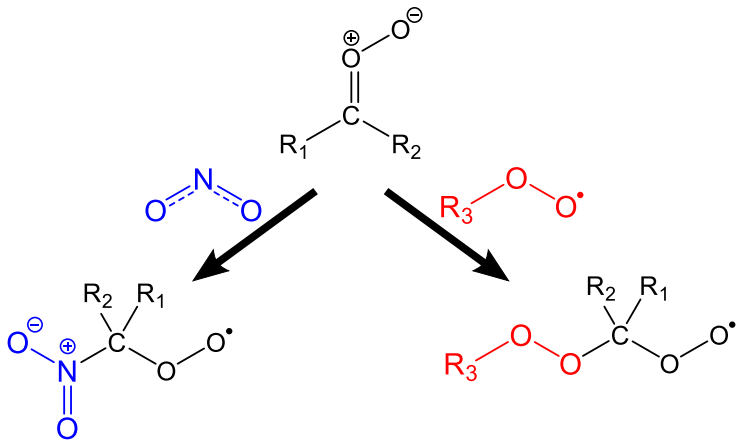

Scheme 8. Addition reactions of Criegee intermediates with NO_2 and RO_2 radicals.

Similar to reactions with NO_2, Criegee intermediate have been predicted to undergo addition reactions with RO_2 with submerged barriers [157, 168]. Recently, Chhantyal-Pun et al. [169] measured rate coefficients for reaction of CH_2OO with CH_3O_2 and $CH_3C(O)O_2$ of ~3× 10^{-11} and ~5.0 × 10^{-11} cm^3 $molecule^{-1}$ s^{-1} at 293 K. Both rate coefficients were found to have a negative temperature dependence with values of (2-10) × 10^{-11} cm^3 $molecule^{-1}$ s^{-1} in the 310-240 K temperature range, consistent with the prediction of a submerged barrier. The adduct product from the reaction of the Criegee intermediate and peroxy radical is also predicted to be a peroxy radical (Scheme 8), which can further react with Criegee intermediates to form oligomerization products with Criegee intermediate units. Zhao et al. [170] observed such oligomers, as shown in Figure 16, with Criegee intermediate units to be the dominant components of SOA formed following the ozonolysis of trans-3-butene. The oligomers were postulated to be formed from sequential addition reaction of RO_2 with Criegee intermediates reactions, as in previous studies [171]. The larger oligomers (n≥4) were dominant in smaller particles, while smaller oligomers (n<4) were abundant in larger particles, suggesting that the oligomers act as nucleating species, and shorter-chain oligomers condense onto existing particles to drive particle growth.

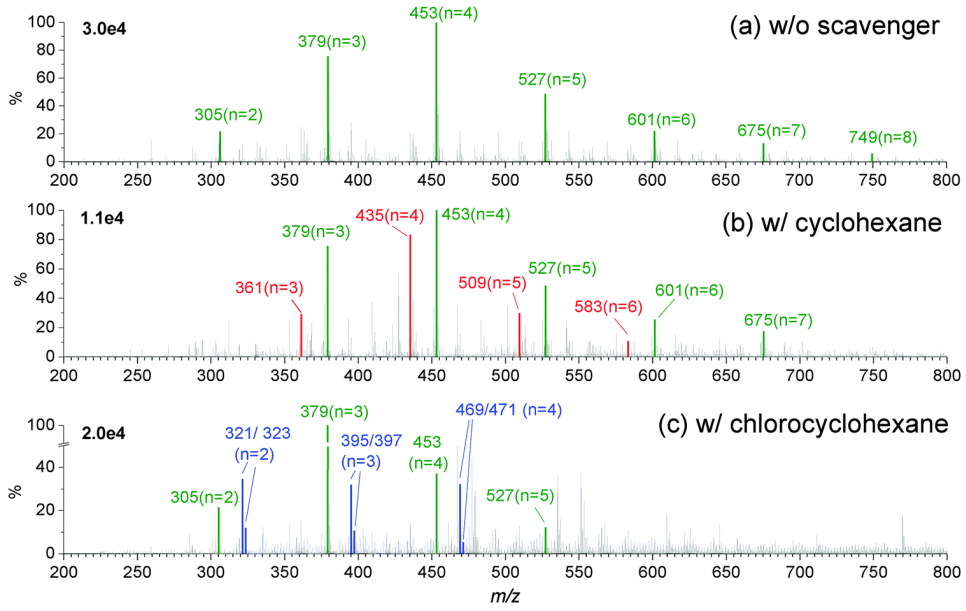

Figure 16. Electrospray ionization mass spectra of SOA produced from ozonolysis of trans-3-hexene showing oligomers with various number of Criegee intermediate units. Different peroxy radicals are produced in the presence of cyclohexane and chlorocyclohexane producing different oligomer mass series. Figure reprinted from Reference [170] with permission from the PCCP Owner Societies.

The adduct peroxy radicals once formed are expected to follow a similar tropospheric fate as other peroxy radicals, i.e. reactions with other peroxy radicals, HO_2 or NO depending on the environment. Reaction with other peroxy radicals and NO will lead to formation of alkoxy

radical which will likely decompose to form smaller products, whereas reaction with HO_2 can form stable MFOHPs. The MFOHPs produced from larger peroxy adducts can condense into secondary organic aerosol as shown in Scheme 5. The combined global chemistry transport modelling and box modelling studies of Chhantyal-Pun et al. [169] showed maximum contributions of ≤3% to the SOA concentration in the Amazon region from reactions of Criegee intermediates with peroxy radicals. The fast reaction of Criegee intermediates with peroxy radicals could also be important in atmospheric simulation chamber experiments. Chamber ozonolysis experiments use OH radical scavengers such as cyclohexane and propane which produce peroxy radicals and unintentionally could also scavenge Criegee intermediates. Thus, the reaction of Criegee intermediate with peroxy radicals should be considered in any reaction model used for estimating product yields from reactions of stabilized Criegee intermediates.

5. Conclusions

Recent advances in the production and detection of Criegee intermediates have allowed direct study of reaction kinetics with a range of tropospherically relevant molecules. These laboratory measurements, interpreted with the aid of computational studies, have revealed some unusual kinetics and reaction mechanisms. Product studies have shown formation of adduct molecules from insertion and addition reactions which can condense into secondary organic aerosols. Similarly, cycloaddition reactions with SO_2 produce SO_3 which is a precursor for sulfate aerosols in the troposphere. Systematic studies of product yields are still lacking and need to be pursued to quantify the importance of these reactions in the troposphere. Similarly, direct studies of larger Criegee intermediates, produced from the ozonolysis of biogenic alkenes, are still rare, but the development of structure activity relationships will help to predict their reactivities for tropospheric modelling studies.

Acknowledgements

We thank NERC (grants NE/K004905/1, NE/P013104/1 and NE/K005316/1), the Primary Science Teaching Trust and Bristol ChemLabS under whose auspices various aspects of this work were funded. We acknowledge Dr. Max McGillen and undergraduate project students Anthony Davey, Lucy Blacker, Matilda Ashcroft, Henry Hill, Aidan Ingham, Marta Duchi, Laura McMahon, Callum Wong, Nick Zachhuber, Rebecca Martin and Sophie Barrington at the University of Bristol for their contributions to reaction kinetic studies. CJP work was carried out at Jet Propulsion Laboratory, California Institute of Technology, under contract with the National Aeronautics and Space Administration (NASA), and was supported by the

Upper Atmosphere Research and Tropospheric Chemistry Programs. The participation of CAT is supported by the Office of Chemical Sciences, Geosciences, and Biosciences, Office of Basic Energy Sciences, United States Department of Energy. Sandia National Laboratories is a multi-mission laboratory managed and operated by National Technology and Engineering Solutions of Sandia, LLC., a wholly owned subsidiary of Honeywell International, Inc., for the U.S. Department of Energy's National Nuclear Security Administration under contract DE-NA0003525 (The Advanced Light Source is supported by the Director, Office of Science, Office of Basic Energy Sciences, of the U.S. Department of Energy under Contract No. DE-AC02-05CH11231). The views expressed in the article do not necessarily represent the views of the U.S. Department of Energy or the United States Government. We are grateful for helpful discussion with Dr. Leonid Sheps.

References

[1] R. Criegee, Angew. Chem. Int. Ed. **14**, 745-752, (1975).
[2] O. Welz, J. D. Savee, D. L. Osborn, S. S. Vasu, C. J. Percival, D. E. Shallcross and C. A. Taatjes, Science **335**, 204-207, (2012).
[3] O. Welz, A. J. Eskola, L. Sheps, B. Rotavera, J. D. Savee, A. M. Scheer, D. L. Osborn, D. Lowe, A. M. Booth, P. Xiao, M. A. H. Khan, C. J. Percival, D. E. Shallcross and C. A. Taatjes, Angew. Chem. Int. Ed. **53**, 4547-4550, (2014).
[4] C. A. Taatjes, O. Welz, A. J. Eskola, J. D. Savee, D. L. Osborn, E. P. F. Lee, J. M. Dyke, D. W. K. Mok, D. E. Shallcross and C. J. Percival, Phys. Chem. Chem. Phys. **14**, 10391-10400, (2012).
[5] R. Chhantyal-Pun, O. Welz, J. D. Savee, A. J. Eskola, E. P. F. Lee, L. Blacker, H. R. Hill, M. Ashcroft, M. A. H. Khan, G. C. Lloyd-Jones, L. Evans, B. Rotavera, H. Huang, D. L. Osborn, D. K. W. Mok, J. M. Dyke, D. E. Shallcross, C. J. Percival, A. J. Orr-Ewing and C. A. Taatjes, J. Phys. Chem. A **121**, 4-15, (2017).
[6] E. Grosjean and D. Grosjean, Atmos. Environ. **30**, 4107-4113, (1996).
[7] E. Grosjean and D. Grosjean, Environ. Sci. Technol. **30**, 2036-2044, (1996).
[8] E. Grosjean, J. B. d. Andrade and D. Grosjean, Environ. Sci. Technol. **30**, 975-983, (1996).
[9] A. R. Rickard, D. Johnson, C. D. McGill and G. Marston, J. Phys. Chem. A **103**, 7656-7664, (1999).
[10] O. Horie and G. K. Moortgat, Atmos. Environ. **25**, 1881-1896, (1991).
[11] C. Schäfer, O. Horie, J. N. Crowley and G. K. Moongat, Geophys. Res. Lett. **24**, 1611-1614, (1997).
[12] R. Wegener, T. Brauers, R. Koppmann, S. R. Bares, F. Rohrer, R. Tillmann, A. Wahner, A. Hansel and A. Wisthaler, J. Geophys. Res. **112**, D13301, (2007).
[13] E. C. Tuazon, S. M. Aschmann, J. Arey and R. Atkinson, Environ. Sci. Technol. **31**, 3004-3009, (1997).
[14] J. T. Herron, R. I. Martinez and R. E. Huie, Int. J. Chem. Kinet. **14**, 201-224, (1982).
[15] S. Hatakeyama, H. Kobayashi, Z.-Y. Lin, H. Takagi and H. Akimoto, J. Phys. Chem. **90**, 4131-4135, (1986).
[16] M. Olzmann, E. Kraka, D. Cremer, R. Gutbrod and S. Andersson, J. Phys. Chem. A **101**, 9421-9429, (1997).

[17] J. D. Fenske, A. S. Hasson, S. E. Paulson, K. T. Kuwata, A. Ho and A. N. Houk, J. Phys. Chem. A **104**, 7821-7833, (2000).
[18] C. A. Taatjes, G. Meloni, T. M. Selby, A. J. Trevitt, D. L. Osborn, C. J. Percival and D. E. Shallcross, J. Am. Chem. Soc. **130**, 11883-11885, (2008).
[19] C. A. Taatjes, O. Welz, A. J. Eskola, J. D. Savee, A. M. Scheer, D. E. Shallcross, B. Rotavera, E. P. F. Lee, J. M. Dyke, D. K. W. Mok, D. L. Osborn and C. J. Percival, Science **340**, 177-180, (2013).
[20] C. C. Womack, M.-A. Martin-Drumel, G. G. Brown, R. W. Field and M. C. McCarthy, Sci. Adv. **1**, e1400105, (2015).
[21] T. Berndt, H. Herrmann and T. Kurtén, J. Am. Chem. Soc. **139**, 13387-13392, (2017).
[22] D. L. Osborn and C. A. Taatjes, Int. Rev. Phys. Chem. **34**, 309-360, (2015).
[23] Y.-P. Lee, J. Chem. Phys. **143**, 020901, (2015).
[24] J. J.-M. Lin and W. Chao, Chem. Soc. Rev. **46**, 7483-7497, (2017).
[25] C. A. Taatjes, Annu. Rev. Phys. Chem. **68**, 183-207, (2017).
[26] M. A. H. Khan, C. J. Percival, R. L. Caravan, C. A. Taatjes and D. E. Shallcross, Environ. Sci: Processes Impacts **20**, 437-453, (2018).
[27] M. I. Lester and S. J. Klippenstein, Acc. Chem. Res. **51**, 978-985, (2018).
[28] D. Johnson and G. Marston, Chem. Soc. Rev. **37**, 699-716, (2008).
[29] G. T. Drozd, T. Kurtén, N. M. Donahue and M. I. Lester, J. Phys. Chem. A **121**, 6036-6045, (2017).
[30] J. G. Calvert, R. Atkinson, J. A. Kerr, S. Madronich, G. K. Moortgat, T. J. Wallington and G. Yarwood, *The Mechanism of Atmospheric Oxidation of the Alkenes*, (Oxford University Press, New York, USA, 2000), p. 1-552.
[31] R. Yajima, Y. Sakamoto, S. Inomata and J. Hirokawa, J. phys. Chem. A **121**, 6440-6449, (2017).
[32] S. Hatakeyama, H. Kobayashi and H. Akimoto, J. Phys. Chem. **88**, 4736-4739, (1984).
[33] A. S. Hasson, G. Orzechowska and S. E. Paulson, J. Geophys. Res. **106(D24)**, 34131-34142, (2001).
[34] M. S. Alam, M. Camredon, A. R. Rickard, T. Carr, K. P. Wyche, K. E. Hornsby, P. S. Monks and W. J. Bloss, Phys. Chem. Chem. Phys. **13**, 11002-11015, (2011).
[35] P. Neeb, O. Horie and G. K. Moortgat, Int. J. Chem. Kinet. **28**, 721-730, (1996).
[36] P. Neeb, O. Horie and G. K. Moortgat, J. Phys. Chem. A **102**, 6778-6785, (1998).
[37] O. Horie, C. Schafer and G. K. Moortgat, Int. J. Chem. Kinet. **31**, 261-269, (1999).
[38] H. Niki, P. D. Maker, C. M. Savage and L. P. Breltenbach, J. Phys. Chem. **85**, 1024-1027, (1981).
[39] C. S. Kan, F. Su, J. G. Calvert and J. H. Shaw, J. Phys. Chem. **85**, 2359-2363, (1981).
[40] F. Su, J. G. Calvert and J. H. Shaw, J. Phys. Chem. **84**, 239-246, (1980).
[41] T. Berndt, J. Voigtländer, F. Stratmann, H. Junninen, R. L. M. III, M. Sipilä, M. Kulmala and H. Herrmann, Phys. Chem. Chem. Phys. **16**, 19130-19136, (2014).
[42] P. Neeb, F. Sauer, O. Horie and G. K. Moortgat, Atmos. Environ. **31**, 1417-1423, (1997).
[43] M. J. Newland, A. R. Rickard, M. S. Alam, L. Vereecken, A. Muñoz, M. Ródenas and W. J. Bloss, Phys. Chem. Chem. Phys. **17**, 4076-4088, (2015).
[44] T. L. Nguyen, H. Lee, D. A. Matthews, M. C. McCarthy and J. F. Stanton, J. Phys. Chem. A **119**, 5524-5533, (2015).
[45] B. J. Finlayson-Pitts and J. N. Pitts, *Chemistry of the upper and lower atmosphere*, (Academic Press, 2000), p. 1-969.
[46] A. S. Hasson, A. W. Ho, K. T. Kuwata and S. E. Paulson, J. Geophys. Res. **106(D24)**, 34143-34153, (2001).
[47] T. Berndt, T. Jokinen, R. L. Mauldin, T. Petäjä, H. Herrmann, H. Junninen, P. Paasonen, D. R. Worsnop and M. Sipilä, J. Phys. Chem. Lett. **3**, 2892-2896, (2012).
[48] H. Niki, P. D. Maker, C. M. Savage, L. P. Breitenbach and M. D. Hurley, J. Phys. Chem. **91**, 941-946, (1987).

[49] T. Berndt, T. Jokinen, M. Sipilä, R. L. M. III, H. Herrmann, F. Stratmann, H. Junninen and M. Kulmala, Atmos. Environ. **89**, 603-612, (2014).
[50] J. P. Hakala and N. M. Donahue, J. Phys. Chem. A **120**, 2173-2178, (2016).
[51] R. A. Cox and S. A. Penkett, J. Chem. Soc., Faraday Trans. 1 **68**, 1735-1753, (1972).
[52] H. Niki, P. D. Maker, C. M. Savage and L. P. Breitenbach, Chem. Phys. Lett. **46**, 327-330, (1977).
[53] M. Sipilä, T. Jokinen, T. Berndt, S. Richters, R. Makkonen, N. M. Donahue, R. L. M. III, T. Kurtén, P. Paasonen, N. Sarnela, M. Ehn, H. Junninen, M. P. Rissanen, J. Thornton, F. Stratmann, H. Herrmann, D. R. Worsnop, M. Kulmala, V.-M. Kerminen and T. Petäjä, Atmos. Chem. Phys. **14**, 12143-12153, (2014).
[54] M. J. Newland, A. R. Rickard, T. Sherwen, M. J. Evans, L. Vereecken, A. Muñoz, M. Ródenas and W. J. Bloss, Atmos. Chem. Phys. **18**, 6095-6120, (2018).
[55] S. E. Paulson and J. H. Seinfeld, Environ. Sci. Technol. **26**, 1165-1173, (1992).
[56] D. Zhang and R. Zhang, J. Chem. Phys. **122**, 114308, (2005).
[57] D. Kotizias, K. Fytianos and F. Geiss, Atmos. Environ. **24A**, 2127-2132, (1990).
[58] Y. Ma and G. Marston, Phys. Chem. Chem. Phys. **10**, 6115-6126, (2008).
[59] J. Ahrens, P. T. M. Carlsson, N. Hertl, M. Olzmann, M. Pfeifle, J. L. Wolf and T. Zeuch, Angew. Chem. Int. Ed. **53**, 715-719, (2014).
[60] R. Winterhalter, P. Neeb, D. Grossmann, A. Kolloff, O. Horie and G. Moortgat, J. Atmos. Chem. **35**, 165-197, (2000).
[61] T. L. Nguyen, J. Peeters and L. Vereecken, Phys. Chem. Chem. Phys. **11**, 5643-5656, (2009).
[62] R. Asatryan and J. W. Bozzelli, Phys. Chem. Chem. Phys. **10**, 1769-1780, (2008).
[63] L. Sheps, J. Phys. Chem. Lett **4**, 4201−4205, (2013).
[64] W.-L. Ting, Y.-H. Chen, W. Chao, M. C. Smith and J. J.-M. Lin, Phys. Chem. Chem. Phys. **16**, 10438-10443, (2014).
[65] D. Stone, M. Blitz, L. Daubney, T. Ingham and P. W. Seakins, Phys. Chem. Chem. Phys. **15**, 19119-19124, (2013).
[66] R. Chhantyal-Pun, A. Davey, D. E. Shallcross, C. J. Percival and A. J. Orr-Ewing, Phys. Chem. Chem. Phys. **17**, 3617-3626, (2015).
[67] Z. J. Buras, R. M. I. Elsamra and W. H. Green, J. Phys. Chem. Lett **5**, 2224-2228, (2014).
[68] E. S. Foreman, K. M. Kapnas and C. Murray, Angew. Chem. Int. Ed. **55**, 10419-10422, (2016).
[69] J. M. Beames, F. Liu, L. Lu and M. I. Lester, J. Am. Chem. Soc. **134**, 20045−20048, (2012).
[70] M. Nakajima and Y. Endo, J. Chem. Phys. **139**, 101103, (2013).
[71] M. C. Smith, W. L. Ting, C. H. Chang, K. Takahashi, K. A. Boering and J. J. M. Lin, J. Chem. Phys. **141**, 074302, (2014).
[72] L. Sheps, A. M. Scully and K. Au, Phys. Chem. Chem. Phys. **16**, 26701-26706, (2014).
[73] J. M. Beames, F. Liu, L. Lu and M. I. Lester, J. Chem. Phys. **138**, 244307, (2013).
[74] F. Liu, J. M. Beames, A. M. Green and M. I. Lester, J. Phys. Chem. A **118**, 2298-2306, (2014).
[75] H.-L. Huang, W. Chao and J. J.-M. Lin, Proc. Natl. Acad. USA **112**, 10857-10862, (2015).
[76] Y. H. Huang, L. W. Chen and Y. P. Lee, J. Phys. Chem. Lett. **6**, 4610-4615, (2015).
[77] V. P. Barber, S. Pandit, A. M. Green, N. Trongsiriwat, P. J. Walsh, S. J. Klippenstein and M. I. Lester, J. Am. Chem. Soc. **140**, 10866-10880, (2018).
[78] M. F. Vansco, B. Marchetti, N. Trongsiriwat, T. Bhagde, G. Wang, P. J. Walsh, S. J. Klippenstein and M. I. Lester, J. Am. Chem. Soc. **141**, 15058-15069, (2019).
[79] C. A. Taatjes, D. E. Shallcross and C. J. Percival, Phys. Chem. Chem. Phys. **16**, 1704-1718, (2014).
[80] T. R. Lewis, M. A. Blitz, D. E. Heard and P. W. Seakins, Phys. Chem. Chem. Phys. **17**, 4859-4863, (2015).
[81] Y.-T. Su, Y.-H. Huang, H. A. Witek and Y.-P. Lee, Science **340**, 174-176, (2013).
[82] F. Liu, J. M. Beames, A. S. Petit, A. B. McCoy and M. I. Lester, Science **345**, 1596-1598, (2014).

[83] M. C. McCarthy, L. Cheng, K. N. Crabtree, J. Oscar Martinez, T. L. Nguyen, C. C. Womack and J. F. Stanton, J. Phys. Chem. Lett. **4**, 4133-4139, (**2013**).
[84] A. M. Daly, B. J. Drouin and S. Yu, J. Mol. Spec. **297**, 16-20, (2014).
[85] C. Giorio, S. J. Campbell, M. Bruschi, F. Tampieri, A. Barbon, A. Toffoletti, A. Tapparo, C. Paijens, A. J. Wedlake, P. Grice, D. J. Howe and M. Kalberer, J. Am. Chem. Soc. **139**, 3999-4008, (2017).
[86] E. S. Foreman, K. M. Kapnas, Y. Jou, J. Kalinowski, D. Feng, R. B. Gerber and C. Murray, Phys. Chem. Chem. Phys. **17**, 32539-32546, (2015).
[87] R. Dawes, B. Jiang and H. Guo, J. Am. Chem. Soc. **137**, 50-53, (2014).
[88] Y.-P. Chang, C.-H. Chang, K. Takahashi and J. J.-M. Lin, Chem. Phys. Lett. **653**, 155-160, (2016).
[89] M. F. Vansco, B. Marchetti and M. I. Lester, J. Chem. Phys. **149**, 244309, (2018).
[90] N. U. M. Howes, Z. S. Mir, M. A. Blitz, S. Hardman, T. R. Lewis, D. Stone and P. W. Seakins, Phys. Chem. Chem. Phys. **20**, 22218-22227, (2018).
[91] Z. J. Buras, R. M. I. Elsamra, A. Jalan, J. E. Middaugh and W. H. Green, J. Phys. Chem. A **118**, 1997-2006, (2014).
[92] L. Sheps, B. Rotavera, A. J. Eskola, D. L. Osborn, C. A. Taatjes, K. Au, D. E. Shallcross, M. A. H. Khan and C. J. Percival, Phys. Chem. Chem. Phys. **19**, 21970-21979, (2017).
[93] R. Chhantyal-Pun, M. R. McGillen, J. M. Beames, M. A. Khan, C. J. Percival, D. E. Shallcross and A. J. Orr-Ewing, Angew. Chem. Int. Ed. **56**, 9044-9047, (2017).
[94] M. R. McGillen, B. F. E. Curchod, R. Chhantyal-Pun, J. M. Beames, N. Watson, M. A. H. Khan, L. McMahon, D. E. Shallcross and A. J. Orr-Ewing, ACS Earth Space Chem. **1**, 664-672, (2017).
[95] H.-Y. Lin, Y.-H. Huang, X. Wang, J. M. Bowman, Y. Nishimura, H. A. Witek and Y.-P. Lee, Nat. Commun. **6**, 7012, (2015).
[96] Y. H. Huang, Y. Nishimura, H. A. Witek and Y. P. Lee, J. Chem. Phys. **145**, 044305, (2016).
[97] Y.-Y. Wang, C.-Y. Chung and Y.-P. Lee, J. Chem. Phys. **145**, 154303, (2016).
[98] P.-L. Luo, Y. Endo and Y.-P. Lee, J. Phys. Chem. Lett. **9**, 4391-4395, (2018).
[99] Y.-P. Chang, H.-H. Chang and J. J.-M. Lin, Phys. Chem. Chem. Phys. **20**, 97-102, (2018).
[100] P.-L. Luo, C.-A. Chung and Y.-P. Lee, Phys. Chem. Chem. Phys. **21**, 17578-17583, (2019).
[101] M. Nakajima, Q. Yue and Y. Endo., J. Mol. Spec. **310**, 109-112, (**2015**).
[102] M. Nakajima and Y. Endo, J. Chem. Phys. **140**, 011101, (2014).
[103] M. Nakajima and Y. Endo, J. Chem. Phys. **145**, 244307, (2016).
[104] J. P. Porterfield, K. L. K. Lee, V. Dell'Isola, P. B. Carroll and M. C. McCarthy, Phys. Chem. Chem. Phys. **21**, 18065-18070, (2019).
[105] C. Cabezas, J.-C. Guillemin and Y. Endo, J. Chem. Phys. **146**, 174304, (2017).
[106] C. Giorio, S. J. Campbell, M. Bruschi, A. T. Archibald and M. Kalberer, Faraday Discuss. **200**, 559-578, (2017).
[107] L. Vereecken, A. Novelli and D. Taraborrelli, Phys. Chem. Chem. Phys. **19**, 31599-31612, (2017).
[108] J. H. Kroll, N. M. Donahue, V. J. Cee, K. L. Demerjian and J. G. Anderson, J. Am. Chem. Soc. **124**, 8518-8519, (2002).
[109] Y. Liu, K. D. Bayes and S. P. Sander, J. Phys. Chem. A **118**, 741-747, (2014).
[110] B. Long, J. L. Bao and D. G. Truhlar, J. Am. Chem. Soc. **138**, 14409-14422, (2016).
[111] T. Berndt, R. Kaethner, J. Voigtlander, F. Stratmann, M. Pfei, P. Reichle, M. Sipila, M. Kulmala and M. Olzmann, Phys. Chem. Chem. Phys. **17**, 19862-19873, (2015).
[112] D. Stone, K. Au, S. Sime, D. J. Medeiros, M. Blitz, P. W. Seakins, Z. Decker and L. Sheps, Phys. Chem. Chem. Phys. **20**, 24940-24954, (2018).
[113] C. A. Taatjes, F. Liu, B. Rotavera, M. Kumar, R. Caravan, D. L. Osborn, W. H. Thompson and M. I. Lester, J. Phys. Chem. A **121**, 16-23, (2017).
[114] Y. Fang, F. Liu, V. P. Barber, S. J. Klippenstein, A. B. McCoy and M. I. Lester, J. Chem. Phys. **144**, 061102, (2016).

[115] M. C. Smith, W. Chao, K. Takahashi, K. A. Boering and J. J.-M. Lin, J. Phys. Chem. A **120**, 4789-4798, (2016).
[116] W. H. Bunnelle, Chem. Rev. **91**, 335-362, (1991).
[117] L. Vereecken, Phys. Chem. Chem. Phys. **19**, 28630-28640, (2017).
[118] S. Jørgensen and A. Gross, J. Phys. Chem. A **113**, 10284-10290, (2009).
[119] J. P. Misiewicz, S. N. Elliott, K. B. M. III and H. F. S. III, Phys. Chem. Chem. Phys. **20**, 7479-7491, (2018).
[120] N. A. I. Watson, J. A. Black, T. M. Stonelake, P. J. Knowles and J. M. Beames, J. Phys. Chem. A **123**, 218-219, (2019).
[121] M. Kumar and J. S. Francisco, Angew. Chem. Int. Ed. **55**, 13432-13435, (2016).
[122] L. Vereecken, A. R. Rickard, M. J. Newland and W. J. Bloss, Phys. Chem. Chem. Phys. **17**, 23847-23858, (2015).
[123] B. Long, J.-R. Cheng, X.-f. Tan and W.-j. Zhang, J. Mol. Struct. Theochem **916**, 159-167, (2009).
[124] R. Chhantyal-Pun, B. Rotavera, M. R. McGillen, M. A. H. Khan, A. J. Eskola, R. L. Caravan, L. Blacker, D. P. Tew, D. L. Osborn, C. J. Percival, C. A. Taatjes, D. E. Shallcross and A. J. Orr-Ewing, ACS Earth Space Chem. **2**, 833-842, (2018).
[125] A. I. Maergoiz, E. E. Nikitin, J. Troe and V. G. Ushakov, J. Chem. Phys. **105**, 6277, (1996).
[126] C. A. Taatjes, M. A. H. Khan, A. J. Eskola, C. J. Percival, D. L. Osborn, T. J. Wallington and D. E. Shallcross, Environ. Sci. Technol. **53**, 1245-1251, (2019).
[127] H. J. Tobias and P. J. Ziemann, J. Phys. Chem. A **105**, 6129-6135, (2001).
[128] R. Chhantyal-Pun, R. J. Shannon, D. P. Tew, R. L. Caravan, M. Duchi, C. Wong, A. Ingham, C. Feldman, M. R. McGillen, M. A. H. Khan, I. O. Antonov, B. Rotavera, K. Ramasesha, D. L. Osborn, C. A. Taatjes, C. J. Percival, D. E. Shallcross and A. J. Orr-Ewing, Phys. Chem. Chem. Phys. **21**, 14042-14052, (2019).
[129] M. Kumar and J. S. Francisco, Phys. Chem. Chem. Phys. **10**, 743-751, (2019).
[130] S. V. Tadayon, E. S. Foreman and C. Murray, J. Phys. Chem. A **122**, 258-268, (2018).
[131] L. McMahon, MSci, University of Bristol, 2017.
[132] D. Lide, *CRC Handbook of Chemistry and Physics: A Ready-Reference Book of Chemical and Physical Data*, 68 edn. (CRC Press, Boca Raton, USA, 2005), p.
[133] Y. Liu, C. Yin, M. C. Smith, S. Liu, M. Chen, X. Zhou, C. Xiao, D. Dai, J. J.-M. Lin, K. Takahashi, W. Dong and X. Yang, Phys. Chem. Chem. Phys. **20**, 29669-29676, (2018).
[134] M. C. Smith, W. Chao, M. Kumar, J. S. Francisco, K. Takahashi and J. J.-M. Lin, J. Phys. Chem. A **121**, 938-945, (2017).
[135] Y.-L. Li, Y.-H. Lin, C. Yin, K. Takahashi, C.-Y. Chiang, Y.-P. Chang and J. J.-M. Lin, J. Phys. Chem. A **123**, 4096-4103, (2019).
[136] W. Chao, C. Yin, K. Takahashi and J. J.-M. Lin, J. Phys. Chem. A **123**, 8336-8348, (2019).
[137] G. J. R. Aroeira, A. S. Abbott, S. N. Elliott, J. M. Turney and I. Henry F. Schaefer, Phys. Chem. Chem. Phys. **21**, 17760-17771, (2019).
[138] Y.-H. Lin, C. Yin, W.-H. Lin, Y.-L. Li, K. Takahashi and J. J.-M. Lin, J. Phys. Chem. Lett. **9**, 7040-7044, (2018).
[139] L.-C. Lin, H.-T. Chang, C.-H. Chang, W. Chao, M. C. Smith, C.-H. Chang, J. J.-M. Lin and K. Takahashi, Phys. Chem. Chem. Phys. **18**, 4557-4568, (2016).
[140] A. B. Ryzhkov and P. A. Ariya, Phys. Chem. Chem. Phys. **6**, 5042-5050, (2004).
[141] D. L. Osborn, P. Zou, H. Johnsen, C. C. Hayden, C. A. Taatjes, V. D. Knyazev, S. W. North, D. S. Peterka, M. Ahmed and S. R. Leone, Rev. Sci. Instrum. **79**, 104103, (2008).
[142] M. Nakajima and Y. Endo, J. Chem. Phys. **140**, 134302, (2014).
[143] C. Cabezas and Y. Endo, ChemPhysChem **18**, 1860-1863, (2017).
[144] C. Cabezas and Y. Endo, Phys. Chem. Chem. Phys. **21**, 18059-18064, (2019).
[145] F. Liu, Y. Fang, M. Kumar, W. H. Thompson and M. I. Lester, Phys. Chem. Chem. Phys. **17**, 20490-20494, (2015).

[146] P. Raghunath, Y.-P. Lee and M. C. Lin, J. Phys. Chem. A **121**, 3871-3878, (2017).
[147] A. C. Rousso, N. Hansen, A. W. Jasper and Y. Ju., Phys. Chem. Chem. Phys. **21**, 7341-7357, (2019).
[148] Y. Sakamoto, S. Inomata and J. Hirokawa, J. Phys. Chem. A **2013**, 12912-12921, (2013).
[149] N. M. Donahue, J. H. Kroll, S. N. Pandis and A. L. Robinson, Atmos. Chem. Phys. **12**, 615-634, (2012).
[150] S. O'Meara, A. M. Booth, M. H. Barley, D. Topping and G. McFiggans, Phys. Chem. Chem. Phys. **16**, 19453-19469, (2014).
[151] M. H. Barley and G. McFiggans, Atmos. Chem. Phys. **10**, 749-767, (2010).
[152] Q. Zhang, J. L. Jimenez, M. R. Canagaratna, J. D. Allan, H. Coe, I. Ulbrich, M. R. Alfarra, A. Takami, A. M. Middlebrook, Y. L. Sun, K. Dzepina, E. Dunlea, K. Docherty, P. F. DeCarlo, D. Salcedo, T. Onasch, J. T. Jayne, T. Miyoshi, A. Shimono, S. Hatakeyama, N. Takegawa, Y. Kondo, J. Schneider, F. Drewnick, S. Borrmann, S. Weimer, K. Demerjian, P. Williams, K. Bower, R. Bahreini, L. Cottrell, R. J. Griffin, J. Rautiainen, J. Y. Sun, Y. M. Zhang and D. R. Worsnop, Geophys. Res. Lett. **34**, L13801, (2007).
[153] S. Enami and A. J. Colussi, Phys. Chem. Chem. Phys. **19**, 17044-17051, (2017).
[154] S. Enami and A. J. Colussi, J. Phys. Chem. A **121**, 5175-5182, (2017).
[155] A. Jalan, J. W. Allenz and W. H. Green, Phys. Chem. Chem. Phys. **15**, 16841-16852, (2013).
[156] L. Vereecken, H. Harder and A. Novelli, Phys. Chem. Chem. Phys. **16**, 4039-4049, (2014).
[157] L. Vereecken, H. Harder and A. Novelli, Phys. Chem. Chem. Phys. **14**, 14682-14695, (2012).
[158] K. T. Kuwata, E. J. Guinn, M. R. Hermes, J. A. Fernandez, J. M. Mathison and K. Huang, J. Phys. Chem. A **119**, 10316-10335, (2015).
[159] R. M. I. Elsamra, A. Jalan, Z. J. Buras, J. E. Middaugh and W. H. Green, Int. J. Chem. Kinet. **48**, 474-488, (2016).
[160] D. Stone, M. Blitz, L. Daubney, N. U. M. Howes and P. Seakins, Phys. Chem. Chem. Phys. **16**, 1139-1149, (2014).
[161] R. Chhantyal-Pun, M. A. H. Khan, R. Martin, N. Zachhuber, Z. J. Buras, C. J. Percival, D. E. Shallcross and A. J. Orr-Ewing, ACS Earth Space Chem. **3**, 2363-2371, (2019).
[162] W.-L. Ting, C.-H. Chang, Y.-F. Lee, H. Matsui, Y.-P. Lee and J. J.-M. Lin, J. Chem. Phys. **141**, 104308, (2014).
[163] Y.-Y. Wang, M. R. Dash, C.-Y. Chung and Y.-P. Lee, J. Chem. Phys. **148**, 064301, (2018).
[164] C. J. Percival, O. Welz, A. J. Eskola, J. D. Savee, D. L. Osborn, D. O. Topping, D. Lowe, S. R. Utembe, A. Bacak, G. McFiggans, M. C. Cooke, P. Xiao, A. T. Archibald, M. E. Jenkin, R. G. Derwent, I. Riipinen, D. W. K. Mok, E. P. F. Lee, J. M. Dyke, C. A. Taatjes and D. E. Shallcross, Faraday Discuss. **165**, 45-73, (2013).
[165] L. Vereecken and H. M. T. Nguyen, Int. J. Chem. Kinet. **49**, 752-760, (2017).
[166] R. L. Caravan, M. A. H. Khan, B. Rotavera, E. Papajak, I. O. Antonov, M.-W. Chen, K. Au, W. Chao, D. L. Osborn, J. J.-M. Lin, C. J. Percival, D. E. Shallcross and C. A. Taatjes, Faraday Discuss. **200**, 313-330, (2017).
[167] B. Ouyang, M. W. McLeod, R. L. Jones and W. J. Bloss, Phys. Chem. Chem. Phys. **15**, 17070-17075, (2013).
[168] J. M. Anglada, S. Olivella and A. Sole, Phys. Chem. Chem. Phys. **15**, 18921-18933, (2013).
[169] R. Chhantyal-Pun, M. A. H. Khan, N. Zachhuber, C. J. Percival, D. E. Shallcross and A. J. Orr-Ewing, ACS Earth Space Chem. , (Submitted).
[170] Y. Zhao, L. M. Wingen, V. r. Perraud, J. Greaves and B. J. Finlayson-Pitts, Phys. Chem. Chem. Phys. **17**, 12500-12514, (2015).
[171] A. Sadezky, R. Winterhalter, B. Kanawati, A. Rompp, B. Spengler, A. Mellouki, G. L. Bras, P. Chaimbault and G. K. Moortgat, Atmos. Chem. Phys. **8**, 2667–2699, (2008).